ESTIMATING GROUND MOTIONS USING RECORDED ACCELEROGRAMS

THOMAS H. HEATON*, FUMIKO TAJIMA**
Dames and Moore, 445 S. Figueroa St., Los Angeles, Calif., U.S.A.
and
ANN WILDENSTEIN MORI***
Exxon Production Research Co., P.O. Box 2189, Houston, Tex., U.S.A.

Abstract. A procedure for estimating ground motions using recorded accelerograms is described. The premise of the study is the assumption that future ground motions will be similar to those observed for similar site and tectonic situations in the past. Direct techniques for scaling existing accelerograms have been developed, based on relative estimates of local magnitude, M_L. Design events are described deterministically in terms of fault dimension, tectonic setting (stress drop), fault distance, and site conditions. A combination of empirical and theoretical arguments is used to develop relationships between M_L and other earthquake magnitude scales. In order to minimize scaling errors due to lack of understanding of the physics of strong ground motion, the procedure employs as few intermediate scaling laws as possible. The procedure conserves a meaningful measure of the uncertainty inherent when predicting ground motions from simple parameterizations of earthquake sources and site conditions.

1. Introduction

The purpose of this review is to present a procedure for estimating strong seismic ground motions that are expected at sites whose tectonic settings and local soil conditions are known. The premise of this study is the assumption that future ground motions will be similar to those which have already been observed in past earthquakes. We seek to find situations with characteristics similar to those found at a site under investigation. To minimize errors due to our poor understanding of the physics of strong ground motion, it is desirable to develop a procedure that employs as few intermediate scaling laws as possible.

This report is a modified version of an in-house manual that was prepared to provide a seismological perspective for those who are faced with problems of design, but who also cannot invest the time to digest and evaluate the large volume of seismological literature concerned with the estimation of strong ground motion. Much of this report is of a review nature and may seem somewhat simplistic to researchers in the fields of both seismology and earthquake engineering. We hope that this report does provide an introductory understanding of the relationship between strong ground motion and earthquake characteristics.

Guzman and Jennings (1976) have described a procedure that is conceptually simple and physically reasonable. They argue that 'design spectra should be established by

Present Address:
* U.S.G.S., Calif, Inst. Tech., Pasadena, Calif., U.S.A.
** Institute for Geophysics, the University of Texas, P.O. Box 7456, Austin, Tex., U.S.A.
*** Seismological Laboratory, Calif. Inst. Tech., Pasadena, Calif., U.S.A.

Surveys in Geophysics **8** (1986) 25-83

direct comparison with the response spectra of existing accelerograms recorded under conditions representative of the postulated earthquake'. Thus, in order to determine expected future motions, we need merely gather and characterize the motions observed for similar earthquakes and site conditions in the past. However, the main problem is that the present data set is too small to encompass the wide variation in tectonic and site conditions that may be encountered. This can be alleviated to some degree by scaling existing records such that they are appropriate for the conditions of a particular design earthquake. Since our understanding of ground motion scaling and of the nature of specific records is poor, it is desirable to keep such scaling procedures to a minimum.

The procedure suggested by Guzman and Jennings (1976) involves scaling records with attenuation laws that are based upon a characterization of peak acceleration. For reasons that will be explained later, we have chosen to scale records with the attenuation law which was developed for use in the local magnitude scale (M_L) by Richter (1958). The engineering significance of the M_L scale has only recently been recognized by Kanamori and Jennings (1978) in their study of the local magnitudes of large events in the western United States. In this study, we extend their results by considering also the local magnitudes of large earthquakes in Japan.

Although Guzman and Jenning's procedure is conceptually very simple, the actual application of the procedure can be confusing and difficult. This is primarily due to the fact that considerable judgment is necessary when this type of procedure is employed. In fact, there seems to be an inherent trade-off between the conceptual simplicity and the tractability for procedures to estimate shaking. As an example, many well-defined procedures consist of the following type of formalism:

$$A(R, M, \omega) = f_1(R) f_2(M) A_0(\omega) \tag{1}$$

where $A(R, M, \omega)$ is the design spectrum, f_1 and f_2 are empirically determined functions of distance and magnitude, and $A_0(\omega)$ is some standard response spectrum that is designed to have the shape of an average record. A procedure that uses this formalism is easy to use since one merely plugs the values into the equation and then obtains the final answer. The major problem with these procedures is that the form of Equation (1) is not defendable. In particular, it is not possible to separate the ground motion into the product of several independent functions. Unfortunately, the problem quickly becomes numerically intractable unless the answer is assumed to have this form.

The procedure that we will demonstrate can be written:

$$A(x_1, \ldots, x_n, \omega) = A_0(x_1^0, \ldots, x_n^0, \omega) f_1(x_1, x_1^0) \ldots f_n(x_n, x_n^0) \tag{2}$$

where $x_1, \ldots, x_n$ are input parameters, A is the design spectrum, A_0 is the observed spectrum at the point $x_1^0, \ldots, x_n^0$, and $f_1, \ldots, f_n$ are scaling laws for each of the parameters. This approximation is best when $(x_i - x_i^0) << x_i^0$, $i = 1, \ldots, n$. Just as in Equation (1), there is no adequate mathematical justification for assuming this form for the function. However, if $(x_i - x_i^0)$ is small, then we can be assured that we are not far from the actual answer. Also, if our parameters, x_i, and their scaling functions are chosen in a physically meaningful way, then there is some chance that the approximation given by

Equation (2) will be meaningful. Unfortunately, many parameters (e.g., the detailed source time history) are virtually indeterminate, and thus, it is difficult for us to ensure that x_i - x_i^0 is small. This is where judgment is important. We must judge the characteristics of both past earthquakes and future ones. Furthermore, since we are commonly confronted with situations for which we have few, if any, historical records, it will often be necessary to make difficult judgments about how to apply past recordings to these new circumstances.

It is clear that when using the type of procedure described by Equation (2), the value of A is quite sensitive to the particular observed spectrum, A_0, which we have chosen to scale. Thus it is important to repeat this procedure in an unbiased way in order to construct a set of scaled design spectra. The final design spectrum is then constructed from this set of scaled observed spectra. The particular manner in which the final design spectrum is constructed depends upon the acceptable level of risk for a particular project.

In order to make the Guzman and Jennings type of procedure useful, we have: (1) summarized the data for past earthquakes; and (2) outlined the way in which these data can be applied to new sites.

2. Engineering Seismology

2.1. The size of earthquakes

The fundamental objective of the procedure to be developed is to translate what is known about faults near a site, to expected strong ground motion at that site. Therefore, some means must be found to characterize earthquakes that are expected to occur on a fault. The most obvious characteristic is the size of the earthquake. Magnitude is the traditional measure of earthquake size, and is the number that is generally passed between geologists and earthquake engineers. The geologist uses studies of fault length versus magnitude to estimate the magnitude of an earthquake on a particular fault. The engineer, using studies of peak acceleration versus magnitude, then selects a ground motion which is based on the magnitude. There are, however, problems associated with this procedure, and these problems can be comprehended through a better understanding of what magnitude means.

Presently, there are several different magnitude scales that can be used to quantify the size of an earthquake. Most of these operate on the assumption that the larger the earthquake, the larger the seismic waves that are radiated. These seismic waves are typically recorded at large distances on different kinds of seismometers. By measuring the size of specific wave types, it is possible to estimate the relative size of earthquakes. The three most commonly used magnitude scales are: M_L, m_b and M_s. The original Richter magnitude scale is M_L and is defined in terms of the logarithm of the maximum amplitude of an earthquake, as recorded by a Wood-Anderson torsion seismometer at distance of 100 km from the source. A distance correction has been included so that the seismometer may lie anywhere within 1000 km of the earthquake. m_b is the body-wave

magnitude and relies upon the amplitudes of body waves (e.g., direct P and S waves) that are recorded at great distances (>2500 km) on a seismometer whose peak amplification is near 1 sec. M_s is the surface wave magnitude and gives an indication of the amplitude of a Rayleigh wave with a period of 20 sec that is recorded at great distance. m_b, M_s and other magnitude scales have been designed such that they are all roughly compatible with the original Richter local magnitude scale. However, the radiation of seismic energy from an earthquake is a very complex process, and it is difficult to know whether these different scales measure the same property of an earthquake. We will later show that in many instances there are important differences between different kinds of magnitude scales. Furthermore, although we know that magnitude gives us some relative measure of size, we do not know exactly what is meant by this vague term, size. For more comprehensive reviews of the magnitude problem, see Båth (1981) and Kanamori (1983).

Much of the original work concerning the physical meaning of magnitude scales centered around the notion of energy. Certainly energy is an excellent candidate for a measure of the size of an earthquake. However, it turns out that energy is a rather difficult quantity to measure and to relate to the actual faulting process; ultimately, we would like to understand what the implications of fault dimensions are in terms of seismic radiation. There are some scaling relationships that can be derived by intuition. Consider a fault plane such as shown in Figure 1. L is the fault length, W is its width, and $\bar{D}$ is the average dislocation of the fault on that surface. Suppose that $U(t)$ is motion recorded at some observation point. If the earth is a linearly elastic system, then $U(t)$ will double if the average dislocation, $\bar{D}$ on the fault surface is doubled. If we were to place two identical earthquakes adjacent to one another, we would effectively double the fault area and $U(t)$ would also double. This example provides the rationale for the

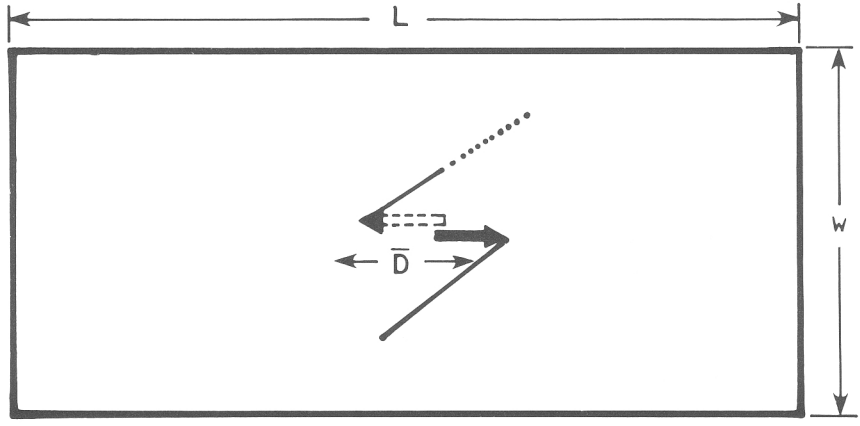

$$M_0 = \mu L W \bar{D}$$

Fig. 1. Definition of seismic moment. μ is the material rigidity in the earthquake source area.

definition of the moment of an earthquake. Moment (M_0) is the basic scaling parameter used in the mathematical modeling of seismic waves radiated by a fault. Moment is defined to be the material rigidity (μ) times the fault area (A) times the average dislocation ($\bar{D}$).

Moment provides a basic link between the dimensions of a fault and seismic waves that are radiated. Thus, a determination of the moment is a convenient way to quantify the size of an earthquake. It is important now to specify the relationship between M_0 and the amplitude of ground motions. This is a difficult task since recorded ground motion depends not only on the overall size of the earthquake, but also upon the specific time history of fault rupture, as well as the particular seismic velocity structure through which the waves travel. However, if there exists a general scaling law between M_0 and the amplitude of seismic waves, it can be used to scale design ground motions. Thatcher and Hanks (1973) pointed out that there is a general relationship between the moments and local magnitudes of southern California earthquakes that is of the form,

$$M_L \cong \frac{\text{Log } M_0 - 16}{1.5}, \tag{3}$$

where M_0 is given in units of dyne-cm. Later, Kanamori (1978) introduced the energy magnitude scale, M_w, which he defined as

$$M_w \cong \frac{\text{Log } W_0 - 11.8}{1.5}, \tag{4}$$

where W_0 is the seismic energy release in ergs. He also noted that, on average, total radiated seismic energy is related to moment by the following relationship.

$$W_0 \cong \frac{M_0}{(2 \times 10^4)}. \tag{5}$$

Substituting (5) into (4), we obtain

$$M_w \cong \frac{\text{Log } M_0 - 16.1}{1.5}. \tag{6}$$

Kanamori defined M_w in this way so that it would be compatible with the energy-magnitude relation developed by Gutenberg and Richter (1956). The energy-magnitude relation was developed using the surface-wave magnitude M_s, for earthquakes in the range $6 < M_s < 8$. Note that relationships (6) and (3) are remarkably similar. Using this observation, Hanks and Kanamori (1979) have introduced the moment magnitude scale, M, which is defined as

$$M \equiv \frac{\text{Log } M_0 - 16.05}{1.5}. \tag{7}$$

Since moment magnitude can be estimated directly from fault area and average dislocation, it provides a convenient quantification of earthquake size. Furthermore, approximate relationships exist between M and more traditional magnitude scales such

as M_L and M_s. However, it is important to recognize that M is conceptually quite different from other magnitude scales in that previous magnitude scales tell us about the amplitude of particular seismic wave types, whereas M is related to actual faulting dimensions. Recently, there has been considerable attention given to the theoretical problem of the relationship between M and other scales such as M_L and M_s. This problem is discussed further in Appendix I.

2.1.1. *Estimation of Moment Magnitude*

We present a simple method for determining the moment of a potential earthquake that is based upon an estimate of the fault dimensions. In the past, estimates of earthquake size, as a function of fault dimension, have been based mostly upon empirical studies of magnitude versus length of surface rupture. The value of such studies is obvious since surface rupture is the most direct measurement of fault dimension possible, and magnitude is the most common measure of the size of an earthquake. Unfortunately, a general misunderstanding of earthquake source processes and earthquake magnitude scales has seriously undermined our ability to obtain physically reasonable results from these studies. It is customary to perform a least squares fit of a straight line to a plot of magnitude versus the logarithm of the fault dimension. This straight line is then used to predict the sizes of future earthquakes based upon the observed lengths of faults. There are problems, however. There is no *a priori* reason to assume that the relationship between the magnitude and the log of the fault dimension is linear. This assumption can lead to difficulties when the relationships are used to extrapolate outside the present data base. For instance, it may be difficult to judge the dimensions of smaller ruptures having minimal surface expressions. Furthermore, the sizes of earthquakes with large rupture dimensions may be poorly represented by traditional magnitude scales due to magnitude saturation phenomena. Finally, it may be that very long ruptures are affected by the properties of deep crustal or mantle rocks, whereas short ruptures are affected by shallow crustal rock properties.

A first requirement is to show how M_0, and thus moment magnitude, can be estimated from a knowledge of rupture length, depth, and the stress drop on the fault. Recall that the definition of moment is,

$$M_0 = \mu A D, \tag{8}$$

where μ is the material rigidity at the source, A is the area of rupture, and $\bar{D}$ is the average dislocation on that area. A can be estimated directly from estimates of the fault dimensions. $\bar{D}$ can be estimated from the average stress drop and the fault geometry. For simplicity, assume that the rupture surface is approximately rectangular, with a length, L, and a width, w. Further assume that the total fault has a length L_0, and a width w_0. Now assume that unless the rupture length is greater than the total fault width, the rupture surface is a square. Therefore,

$$\begin{aligned} w &= w_0; \quad L > w_0. \\ w &= L; \quad L < w_0. \end{aligned} \tag{9}$$

$$M_0 = \frac{w_0^2 L \Delta\sigma}{(C_D - 0.9)}; \quad L > 2w_0 \text{ (long rupture).}$$

The moment magnitude can then be calculated by using Equations (14) and (7).

$$\begin{aligned} M &= 2 \operatorname{Log} L + \tfrac{2}{3} \operatorname{Log} \Delta\sigma - \tfrac{2}{3} \operatorname{Log} C_D - 10.7: \quad L = w < w_0 \\ M &= \tfrac{2}{3} \operatorname{Log} \frac{w_0^2 L}{C_D + 0.9\left(1 - \dfrac{L}{w_0}\right)} + \tfrac{2}{3} \operatorname{Log} \Delta\sigma - 10.7: \quad w_0 < L < 2w_0 \\ M &= \tfrac{4}{3} \operatorname{Log} w_0 + \tfrac{2}{3} \operatorname{Log} \Delta\sigma + \tfrac{2}{3} \operatorname{Log} L - \\ &\quad - \tfrac{2}{3} \operatorname{Log}(C_D - 0.9) - 10.7: \quad L > 2w_0 \end{aligned} \tag{15}$$

where all lengths are given in centimeters (cm), and the stress drop is given in dyne/cm^2. Equation (15) still leaves us with some uncertainty. For example, what is the width of a particular fault and what is the stress drop? For each of these variables, we can only make an educated guess. In California, there do not seem to be earthquakes deeper than 20 km. There, we might choose the fault's width to be 20 km/sin θ (θ is the dip angle), or else equal to the fault's length, whichever is smaller. In Benioff Zones, fault widths can be much larger since earthquake depths are greater. Estimating fault width is a matter of judgment, and its uncertainty reflects a true uncertainty in the problem.

The other uncertain parameter is stress drop. Kanamori and Anderson (1975) have reviewed this problem and they conclude that the worldwide average stress drop is about 30 bars (1 bar $\cong 10^6$ dyne/cm^2). However, this number varies from less than 10 bars to over 100 bars for individual earthquakes. There does appear to be some systematic relationship with respect to tectonic environment. It appears that stress drops may be highest in regions well removed from plate tectonic boundaries. Such earthquakes are called intraplate earthquakes and their average stress drop is about 60 bars. Interplate earthquakes, those associated with non-sunducting plate boundaries, have an average stress drop of about 30 bars. It also appears that shallow interplate subduction-zone earthquakes may have a somewhat lower average stress drop of 15 bars. In general, the stress drop is a very important quantity about which we know disappointingly little.

Despite the uncertainties, Equation (15) provides us with the means to scale earthquake size in a physically meaningful way. In Figure 2 we show the theoretical relationship between moment magnitude and rupture length assuming stress drops of 15, 30, and 60 bars, $C_D = 1.6$ (surface rupture), and two different types of faults. In one case, the fault width is set equal to the fault length. In the other case, the fault width does not exceed 20 km. This second case would simulate a shallow strike-slip environment. Notice that if there is a maximum fault width, then our relationship cannot be expressed in terms of a single straight line. Also, keep in mind that we have plotted rupture length versus moment magnitude. As we will later see, the relationship between moment magnitude and other magnitude scales is not always simple. Thus we may expect the relationship between fault length and traditional magnitudes to be fairly complex.

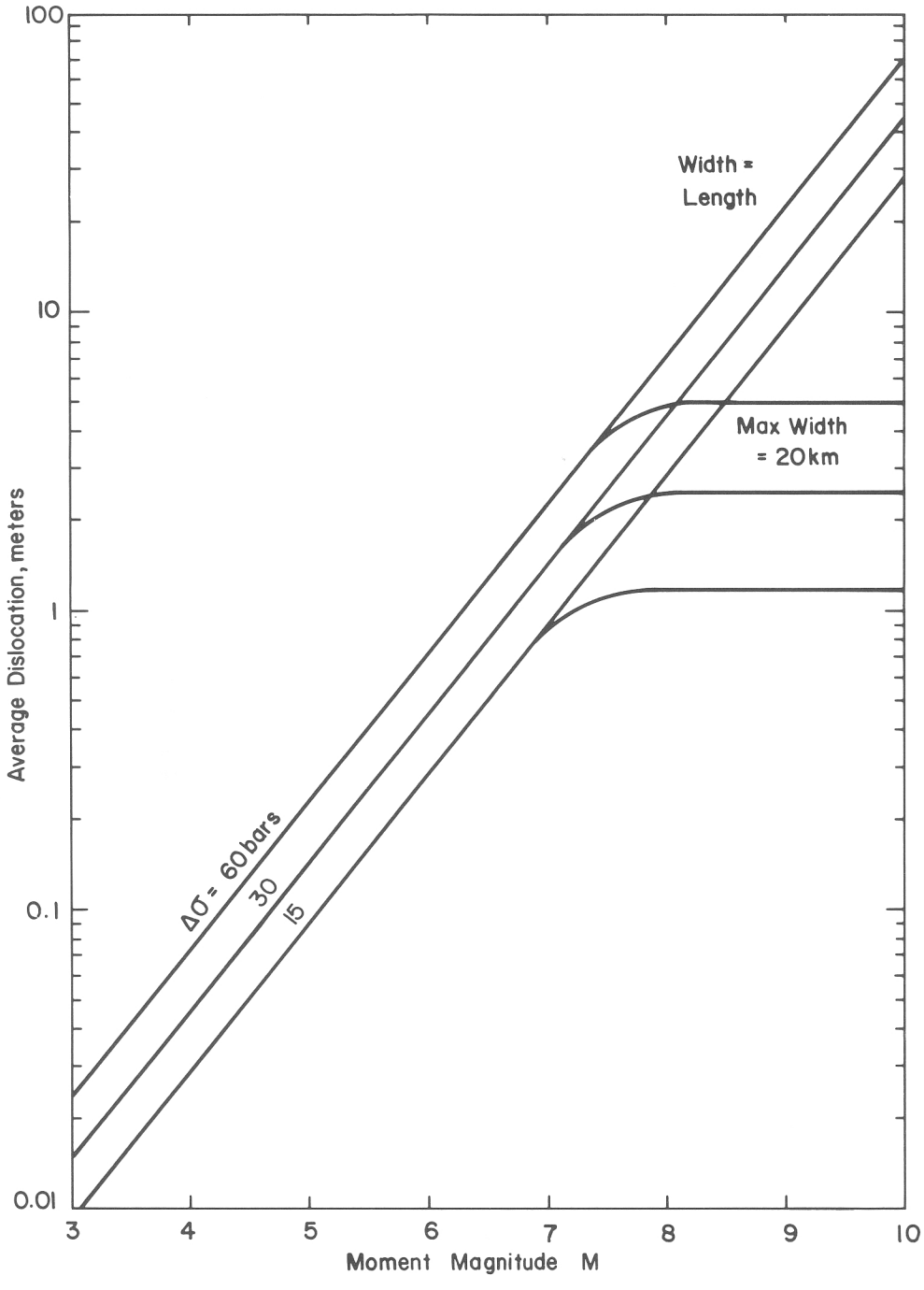

Fig. 2. Moment magnitude given as a function of rupture length as calculated from Equation (15). Straight lines correspond to those cases in which the rupture width is assumed to be equal to the rupture length. Curved lines correspond to cases in which a maximum rupture width of 20 km is assumed. Shallow faulting is assumed and the material rigidity is taken to be 3.5×10^{11} dyne/cm^2.

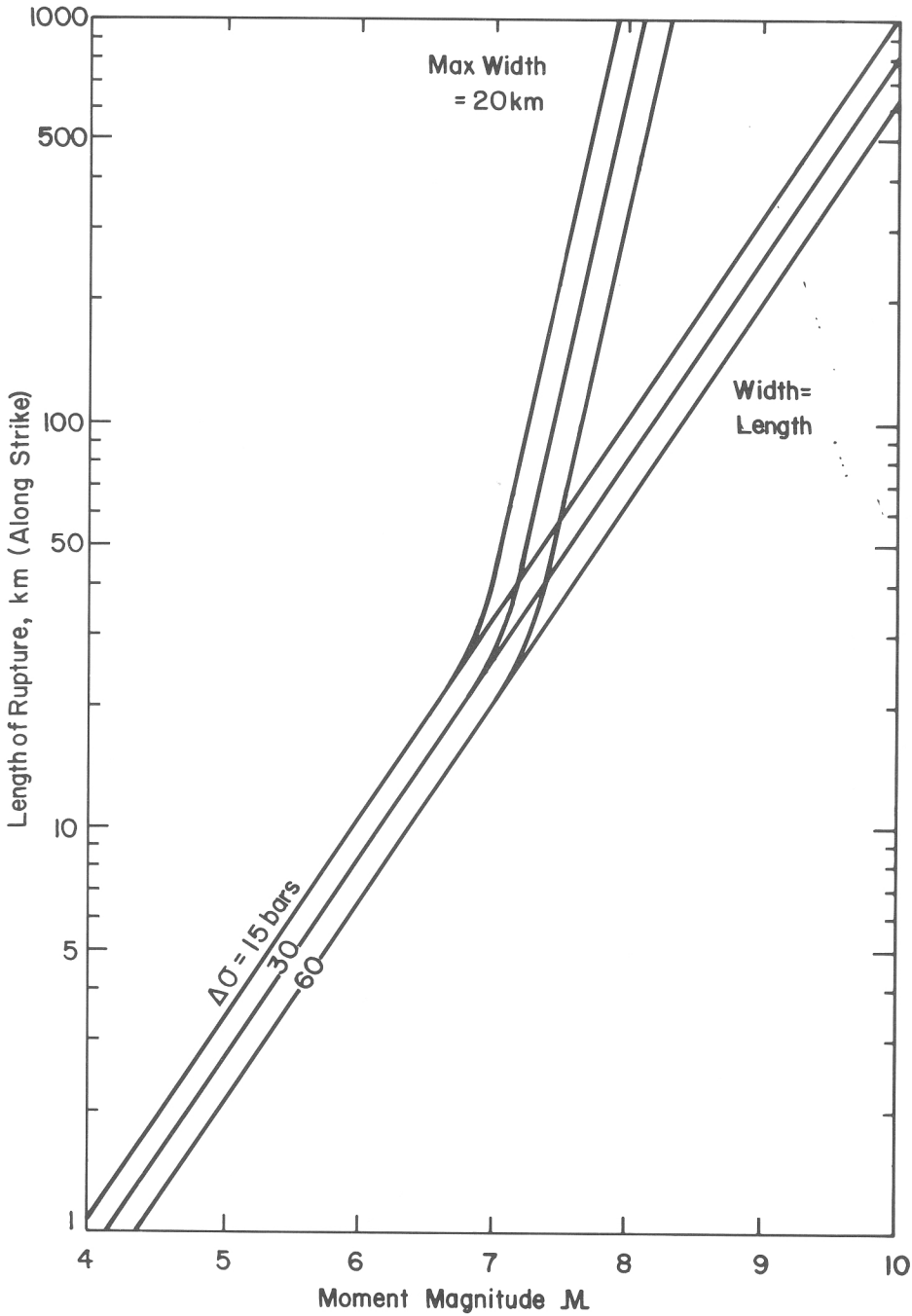

Fig. 3. Average dislocation given as a function of moment magnitude as calculated from Equations (13) and (15). The assumptions used are identical to those used in Figure 2.

In Figure 3 we show the predicted relationship between moment magnitude and average dislocation. Again, we assumed stress drops of 15, 30 and 60 bars and two different cases of fault width. Notice that when the maximum width is fixed, as the fault length becomes much larger than the fault width, the average dislocation tends to a constant value which is determined by the fault width and the stress drop. Also, if the maximum fault width is 20 km, it is unlikely that it will produce an earthquake having a magnitude much larger than 8.

2.1.2. *Relationship Between Moment Magnitude and Other Magnitude Scales*

We have seen that it is very convenient to quantify earthquake size by seismic moment. However, seismic moment alone does not tell us how to scale strong motion amplitudes with fault dimension. Furthermore, seismic moment is a relatively new concept and estimates of this parameter are not available for many earthquakes of interest. In this section we discuss the relationships between moment magnitude and other magnitude scales. The relationships we will show have been developed primarily on the basis of

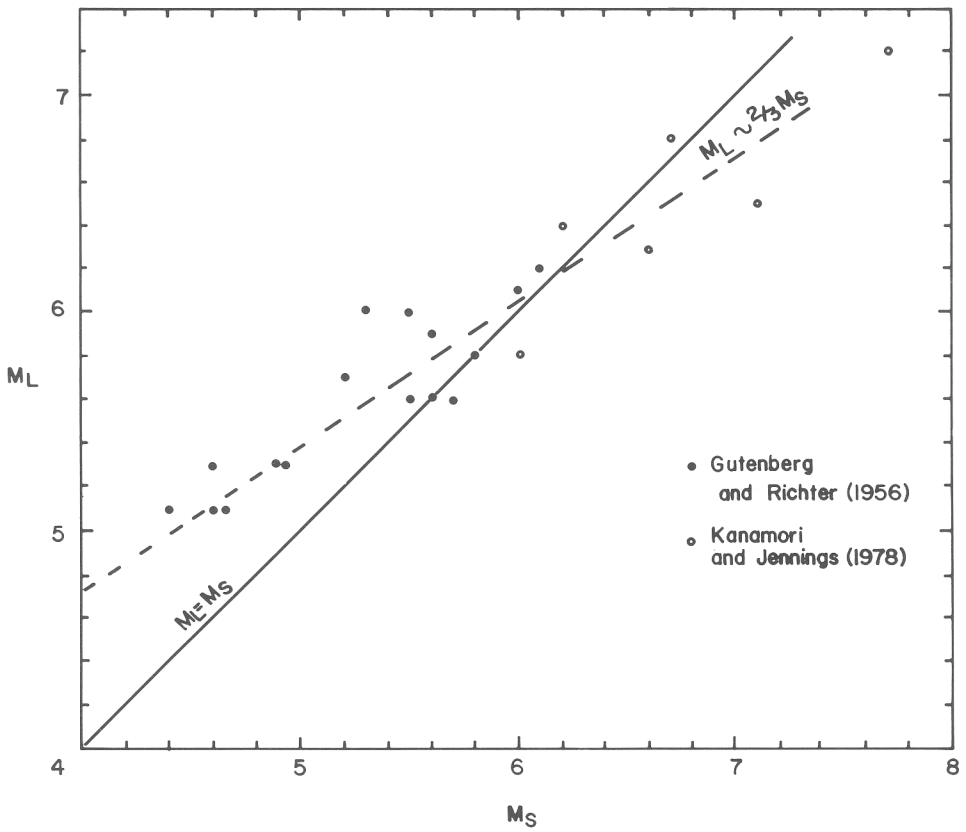

Fig. 4. Plot of observed local magnitudes versus surface wave magnitudes for earthquakes in the western United States.

empirical studies. However, in Appendix I we also discuss the results of theoretical studies of seismic sources which give insight into this problem.

In the last section, we noted that Thatcher and Hanks (1973) and Kanamori (1978) proposed relationships between M and M_L, and M and M_s that are virtually identical. This might lead one to the conclusion that M_L and M_s are equivalent. Indeed, M_s was defined by Gutenberg and Richter (1956) such that M_s is an extension of the local magnitude scale. They used aftershocks of the 1952 Kern County earthquake to calibrate the M_s scale such that these aftershocks gave similar magnitudes on both scales. However, their study only considered earthquakes with magnitudes between 5 and 6. Due to the limited dynamic range of available instruments, M_L was not available

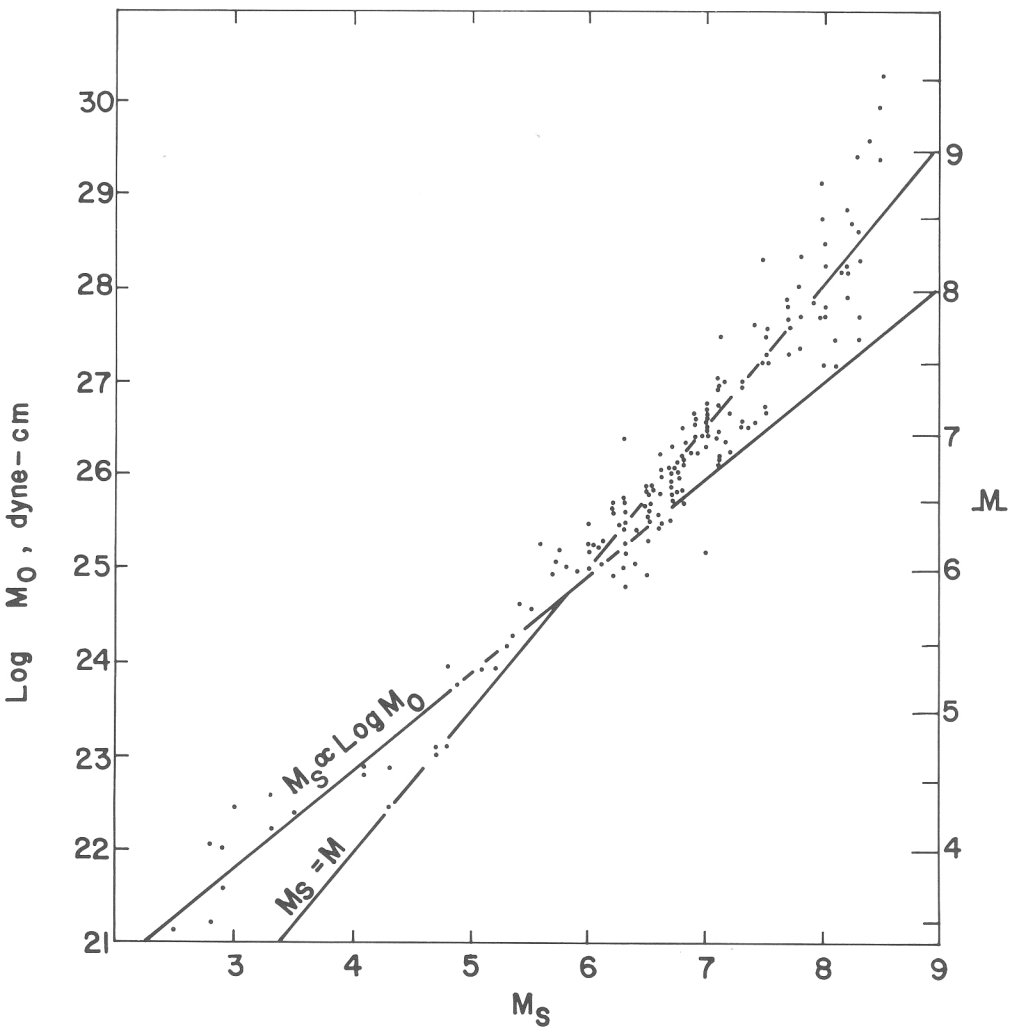

Fig. 5. Plot of surface wave magnitude versus log moment or moment magnitude for world-wide earthquake sample (modified from Purcaru and Berckhemer, 1978).

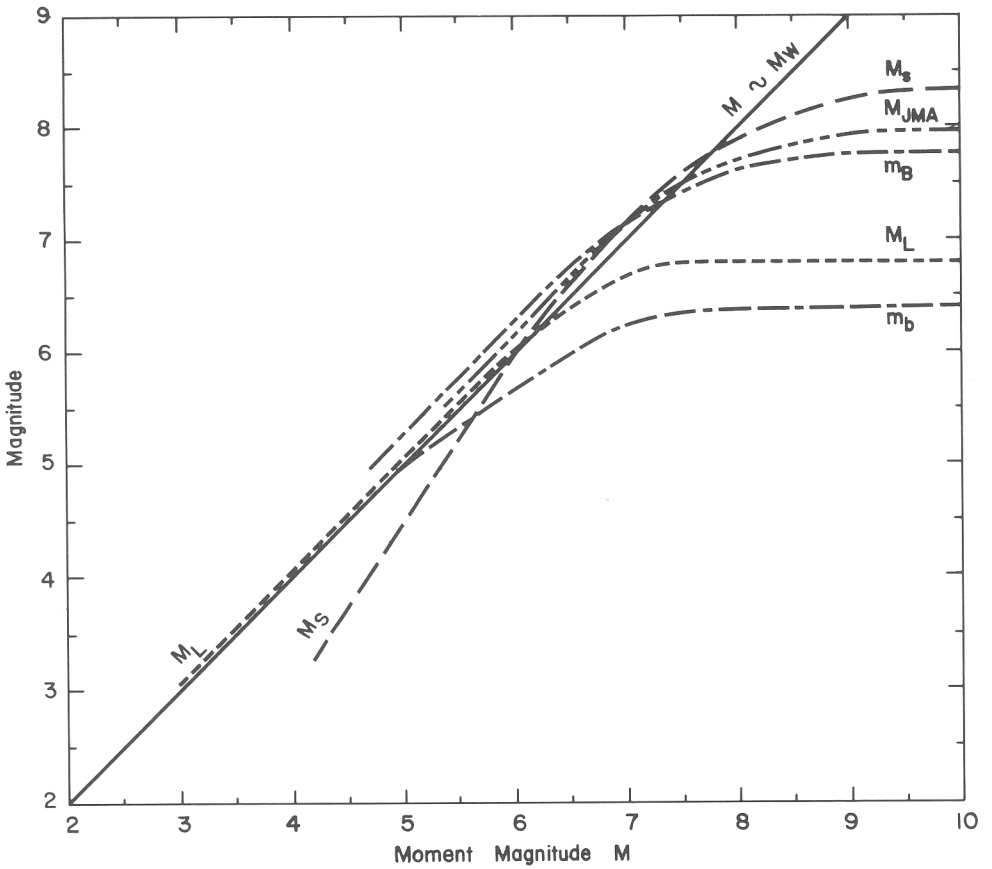

Fig. 6. Comparison of several different magnitude scales with the moment magnitude scale.

for larger earthquakes and M_s was not available for smaller earthquakes. Recently, Kanamori and Jennings (1978) have calculated M_L for larger earthquakes by using strong motion records. In Figure 4 we show a plot of M_L versus M_s using the combined data sets of Gutenberg and Richter (1956) and Kanamori and Jennings (1978). Although the line $M_L = M_s$ runs through many data points, an obvious skew is present in this plot. This is contradictory to our previous conclusion that M_L and M_s are equivalent. Although this may seem somewhat paradoxical, we can better understand the situation by examining a plot of M_s versus log M_0 that was presented by Purcaru and Berckhemer (1978). In Figure 5, we see that between $M_s = 6$ and $M_s = 8$, that $M_s \cong M$. This is in agreement with Kanamori's earlier work. However, for magnitudes less than 6, M_s and M no longer coincide. In Appendix I, we show that this change in slope can be easily explained by theoretical source models. By examining Figures 4 and 5 we can conclude that M_L and M are roughly equivalent up to magnitude 6 and that thereafter, M_L increases more slowly than M.

In Figure 6 we show the relationships between moment magnitude and other

magnitude scales. Our construction of these curves involves the synthesis of many different studies. We began by plotting M_s as a function of moment magnitude using the results of Kanamori and Anderson (1975), which apply for moment magnitudes between 6 and 9, and also the results of Purcaru and Berkhemer (1978) which apply for moment magnitudes between 3 and 9. We used the results of Thatcher and Hanks (1973) to define the relationship between M_L and M for $3 < M < 6$. We then used relationships between M_L and M_s given by Gutenberg and Richter (1956) and by Kanamori and Jennings (1978) to extend the relationship between M_L and M for $M < 6$. The relationship between M_L and M is further corroborated by using relationships between M_L and M_{JMA} (Japan Meterological Agency) that are presented in Appendix II and relationships between M_{JMA} and M_s (Tsuboi, 1954, and also Appendix II). Finally, we were able to obtain m_B (long-period body-wave magnitude) and m_b (short-period body-wave magnitude) as a function of moment magnitude by using relationships between M_s and m_B (Abe and Kanamori, 1980), M_s and m_b (Noguchi and Abe, 1977), and m_B and m_b (Abe, 1981).

There are serveral noteworthy aspects of the relationships shown in Figure 6. All of the magnitude scales exhibit a saturation level with increasing moment magnitude. That is, beyond a certain level, individual magnitude scales no longer reflect the true size of earthquakes. As an example, consider the 1960 Chilean earthquake, the largest known instrumentally recorded earthquake. Aftershock studies indicate that the fault ruptured over an area which is comparable to the surface area of the entire State of California. Kanamori (1978) has estimated the M_0 of this event to be 2×10^{30} dyne-cm. Another well known large earthquake is the 1906 San Francisco earthquake. The fault area for this earthquake, though, was much smaller than that which ruptured in the 1960 Chilean event. The San Francisco event had a M_0 of about 10^{28} dyne-cm, and thus, in terms of moment (and energy), the Chilean event was about 200 times larger than the San Francisco earthquake. Yet, these two earthquakes had virtually identical surface wave magnitudes of $8\frac{1}{4}$. Clearly, the M_s scale fails to give an adequate representation of the size of giant earthquakes. What this means is that beyond a certain magnitude, the amplitudes of 20-sec surface waves do not increase with increasing earthquake size. This phenomenon is referred to as saturation of the magnitude scale. Saturation occurs when the fault dimension becomes much larger than the wave length of seismic waves that are used to determine the magnitude.

The relationship between M and M_L is of great interest since M can be related to fault dimensions, and M_L is a measure of seismic radiation at distances that are close to the source. As was stated before, M_L is a measure of the size of recording made by a Wood-Anderson torsion seismometer. This instrument is actually a single-degree-of-freedom, linear, 80% damped, harmonic oscillator with a free period of 0.8 sec and a gain of 2800. There are two important implications of the characteristics of this instrument: (1) the maximum amplitude, as read on this instrument, gives a point on the response spectrum for that motion at 0.8 sec and 80% damping, and (2) the period at which M_L is measured is much shorter than the period at which M_s is measured. The first implication tells us that M_L provides a scaling of the type of seismic waves that are of interest in

earthquake engineering. The second means that we should expect a saturation of the local magnitude scale even before M_s saturates. Since we intend to use M_L in our procedure for estimating ground motions, the saturation level of M_L is of keen interest. We give a more detailed discussion of this problem in het next section.

There are several other noteworthy features of Figure 6. We can see that both m_B (long-period body-wave magnitude) and M_{JMA} give a fairly good indication of the size of earthquakes having moment magnitudes less than 8. Both of these scales are based upon measurements of peak amplitudes of waves with periods between 5 and 10 sec. m_B is important since it is available for many older earthquakes (see Abe, 1981). Unfortunately, it is not available for most recent events. Due to changes in instrumentation in the 1960's, the m_B scale was replaced by the m_b scale. m_b is based on the amplitude of the initial several seconds of teleseismic body waves with periods near 1 sec. Unfortunately, m_b does not seem to give a very good indication of earthquake size.

2.2. Implications of the local magnitude scale

Although the M_L scale was originally developed to measure the overall size of earthquakes, it has become clear that M_L is well suited to measure the relative sizes of strong ground motions. As a part of the guidelines, we use M_L to scale strong motion records in a very direct manner. A modified version of Richter's original distance function is used to scale records with distance. Records are scaled according to earthquake size by using the definition of the magnitude scale directly. Site effects (the effects of local soils) are included by introducing an appropriate correction factor. Local magnitudes are related to fault dimensions by simple relationships that can be derived from dislocation theory. It is important to recognize that the M_L scale is not a panecea. Most of the problems that are associated with understanding the motions that are produced by a particular earthquake still exist. The conceptual simplicity that results from using the local magnitude scale to estimate response spectra is the major motivation for incorporating local magnitude into our procedure for estimating ground motions.

The definition of local magnitude is,

$$M_L = \text{Log}\, A_{wa} - \text{Log}\, A_0, \tag{16}$$

where A_{wa} is the maximum trace amplitude on a Wood-Anderson (horizontal) seismometer, and A_0 is a distance correction which will be discussed shortly. Now if the displacement response spectrum of a motion is given by $S_d(\tau, \xi)$, where τ is period, and ξ is the damping fraction, then

$$S_d(t = 0.8, \xi = 0.8) = A_{wa}/2800, \tag{17}$$

where the factor of 2800 is included to correct for the gain of a Wood-Anderson seismometer. Combining Equations (16) and (17), we obtain

$$S_d(\tau = 0.8, \xi = 0.8) = \frac{A_0\, 10^{M_L}}{2800}. \tag{18}$$

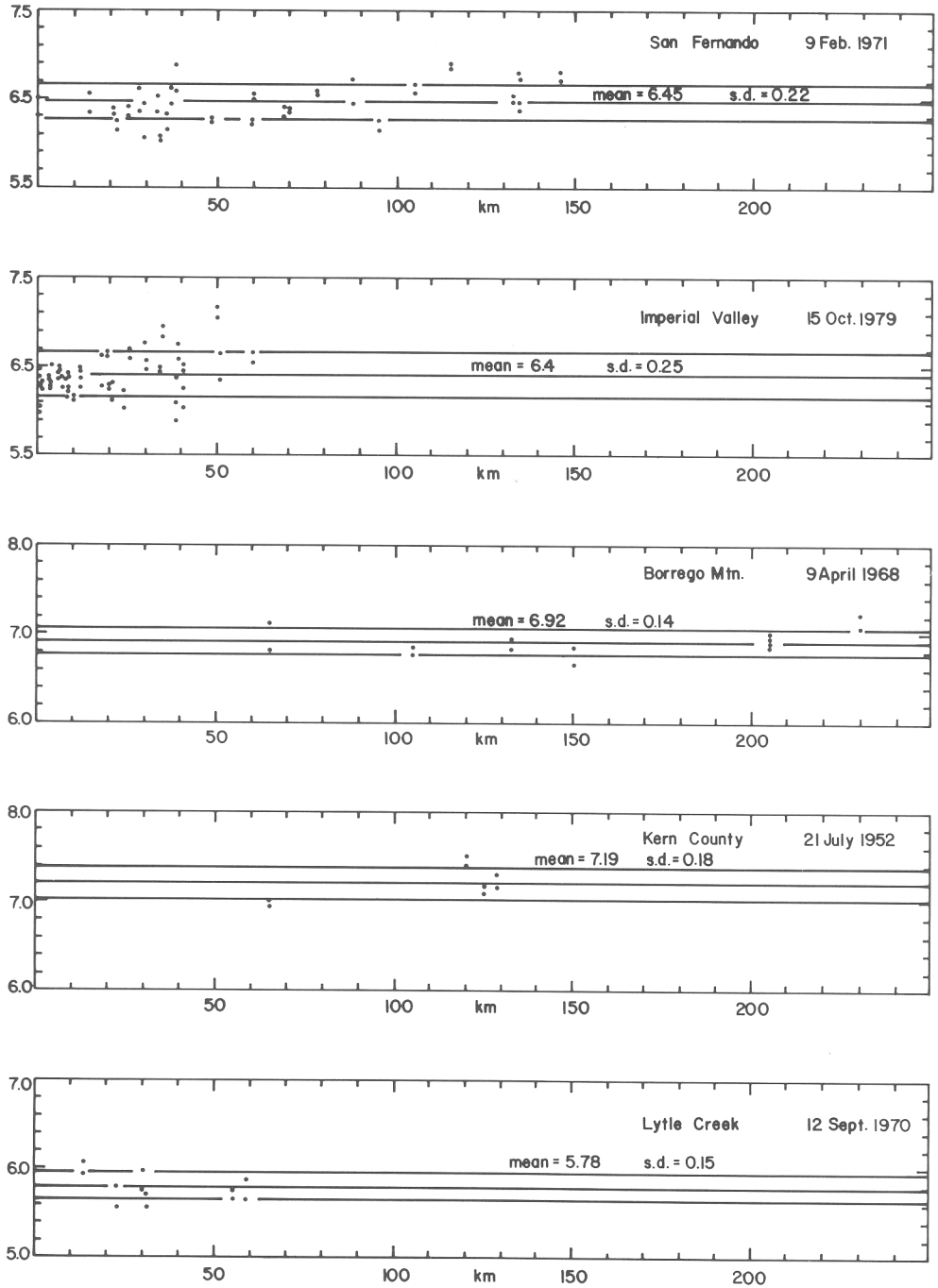

Fig. 7. Values of local magnitude plotted as a function of distance for several California earthquakes. Lines indicate mean values and $\pm$ one standard deviation. The modified distance attenuation factor of Jennings and Kanamori (1982) was assumed and data were taken either from Kanamori and Jennings (1978) or were new data used with the permission of Kanamori and Jennings.

For periods near one second, there is a general correspondence between response spectral level and the peak velocity of the ground motion. In fact, the output of a Wood-Anderson seismometer usually looks very similar in character to records of ground velocity. Thus, the local magnitude scale can be thought of as a scaling relationship for ground velocity. We must now address some important, but difficult, questions concerning the local magnitude scale. How well does the local magnitude scale work when scaling strong ground motions? How well can we estimate the relationships between fault dimensions and local magnitudes? Before discussing these problems, we warn the reader that a full resolution of these questions has not, to date, been possible.

Kanamori and Jennings (1978) have studied the local magnitudes of the larger earthquakes in the western United States, and their results demonstrate the feasibility of using local magnitude as a scaling relationship for strong ground motions. Notice that Equation (16) indicates that the correction for the decay of amplitude with distance is not a function of magnitude. Since Richter originally derived this relationship using small earthquakes, it is not clear whether it also applies to large earthquakes. Kanamori (1978) has pointed out that 'it is possible that, for very large earthquakes, complex interference of seismic waves originating from different parts of the fault plane may significantly affect the decay rate of the maximum amplitude resulting in distance dependent M_L'.

Figure 7, which was constructed from studies by Kanamori and Jennings (1978) and Jennings and Kanamori (1982), shows the value of M_L as a function of distance for several well-recorded California earthquakes. The values of M_L are defined according to the definition given in Equation (16). However, we have used a distance attenuation factor which Jennings and Kanamori (1982) modified from the original one given by

TABLE I

Local magnitude distance attenuation factor
(modified by Jennings and Kanamori, 1983)

Distance (km)	$-\text{Log } A_0$	Distance	$-\text{Log } A_0$
0	1.4	120	3.1
3	1.5	140	3.2
6	1.6	160	3.3
9	1.7	180	3.4
12.5	1.8	200	3.5
16.5	1.9	220	3.6
21	2.0	240	3.7
26	2.1	260	3.8
31	2.2	280	3.9
37	2.3	300	4.0
43	2.4	320	4.1
51	2.5	340	4.2
60	2.6	360	4.3
70	2.7	380	4.4
80	2.8	400	4.5
90	2.9	450	4.6
100	3.0	500	4.7

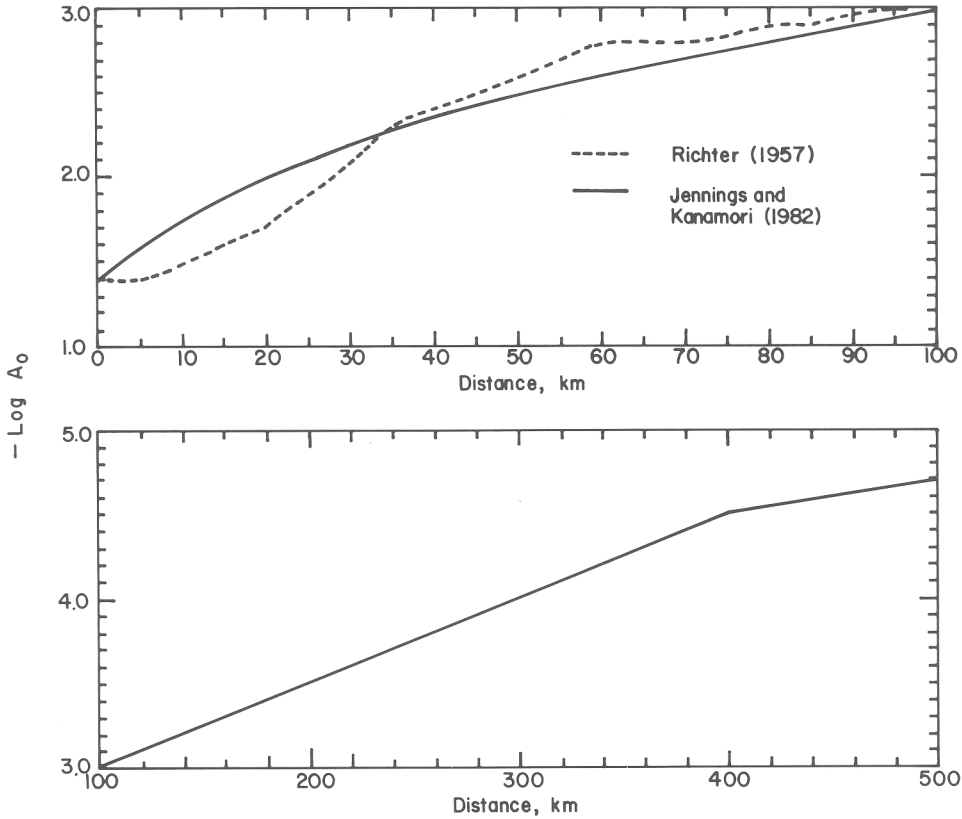

Fig. 8. Distance attenuation laws for local magnitude scale. Dotted line signifies the attenuation law originally proposed by Richter (1958) and the solid line is the modified attenuation law proposed by Jennings and Kanamori (1982).

Richter (1958). Both the original and modified distance attenuation curves are shown in Figure 8. In Figure 7 we see that there are not obvious systematic trends with distance, indicating that the modified attenuation curve is appropriate for strong motion scaling purposes. This new attenuation curve is also compatible with recent simulation studies conducted by Hadley and Helmberger (1980). Throughout the remainder of this study, we will assume that the modified attenuation curve is more appropriate for scaling strong motions. Table I gives values of Log A_0 as a function of distance.

Figure 7 also shows the scatter typically encountered in the measurement of local magnitudes. The degree of scatter for these larger events is not significantly larger than that encountered when studying the local magnitudes of small earthquakes. It should be remembered, however, that the local magnitude scale is logarithmic, and a factor of 2 in amplitude corresponds to a difference in magnitude of only 0.3 units.

At this point, it is instructive to compare the distance scaling in the local magnitude scale with some of the familiar distance scaling laws that have been traditionally used in

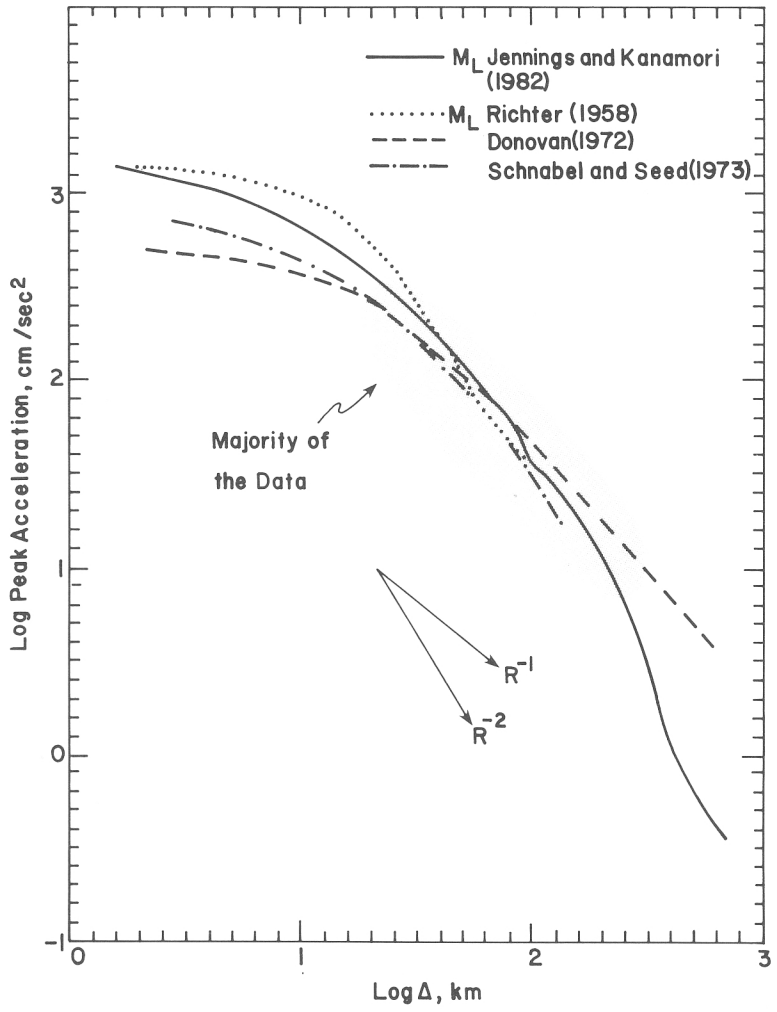

Fig. 9. Comparison of different distance attenuation laws for M 6-1/2 earthquakes (modified from Trifunac and Brady, 1976).

earthquake engineering. Figure 9 shows the distance scaling for M_L along with a variety of other distance scaling laws. Several of these other scaling relationships are for peak acceleration, whereas M_L is more related to a peak velocity relationship. Kanamori and Jennings (1978) were not the first to use local magnitudes in the scaling of strong ground motions. Trifunac and Brady (1976) also used Richter's distance scaling law to scale strong motions with distance. Figure 9 is a modification of Figure 1 in Trifunac and Brady's (1976) paper. A detailed inspection of Figure 9 shows some interesting differences between the M_L scaling and other scaling relationships. Although all of the curves pass through the bulk of the data, Richter's original curve shows a generally higher rate of attenuation in the distance range of 20 to 200 km than the other curves

do. However, in this same distance range, the modified M_L attenuation law shows an attenuation rate that is compatible with the attenuation law for ground velocities proposed by Espinosa (1977). This observation further supports the use of the modified M_L attenuation curve. Although the modified M_L curve shows a more gradual attenuation than the original between 20 and 200 km, it does attain the same high value for zero distance as Richter's original. This value is significantly higher than that predicted from Schnabel and Seed's (1973) or Donovan's (1972) acceleration attenuation curves. However, the scatter in the data is quite large and there are still relatively few data available at very small distances. At present, it does not seem possible to verify the level of shaking that is predicted by the M_L scale at very small distances. However, new data from the 1979 Imperial Valley earthquake tends to support the hypothesis that the M_L distance attenuation curve is indeed appropriate for very small source distances and moderate sized earthquakes. Papers by Trifunac and Brady (1976) and Trifunac (1976) contain enlightening discussions on the use of Richter's distance scaling law.

We now comment on the way in which local magnitude scales amplitude with magnitude. By the definition of local magnitude (Equation (21)), the peak amplitude, as recorded by a Wood-Anderson torsion seismometer, depends exponentially on the local magnitude. That is, for each unit increase in M_L, the response spectrum at 0.8 sec for 80% damping increases by a factor of 10. Although this is a statement of the obvious, the implications are significant. In Figure 10, the expected peak amplitude of a Wood-Anderson recording (approximately related to the peak ground velocity) are plotted as a function of magnitude and distance. For comparison, Schnabel and Seed's (1973) estimation of peak acceleration, as a function of magnitude and distance, is also shown. The difference in the nature of these curves is striking. Not only are the distance attenuation curves different, but the peak accelerations clearly do not depend on magnitude in an exponential fashion. There is a variety of explanations for this.

The first thing to remember is that the local magnitude scale saturates before the surface wave magnitude scale does. Schnabel and Seed's curves are given as a function of M_S, and for magnitudes of 6-1/2 and above, the local magnitude scale does not give a good representation of the overall size of the earthquake. This point was discussed in the last section. Also, Schnabel and Seed's curves are for peak acceleration which is a measure of the amplitudes of high-frequency waves generated by the earthquake. The same phenomenon that is responsible for the saturation of M_L also causes the peak acceleration to saturate, but at a lower magnitude. Trifunac (1976) documents the fact that peak accelerations are a weaker function of earthquake size than peak velocity.

Finally, the relationships shown in Figure 12 are basically empirical in nature. Since there are very few data at small distances or from large earthquakes, both of these sets of curves could be inappropriate for small distances or large earthquakes. In fact, there is good reason to suspect that the M_L scaling law may not be appropriate at small distances and for M_L's above 6-1/2. This can be seen best by examining the local magnitudes of the 1971 San Fernando earthquake. Kanamori and Jennings (1978) determined that the M_L of this earthquake was 6.5. They also found that the accelero-

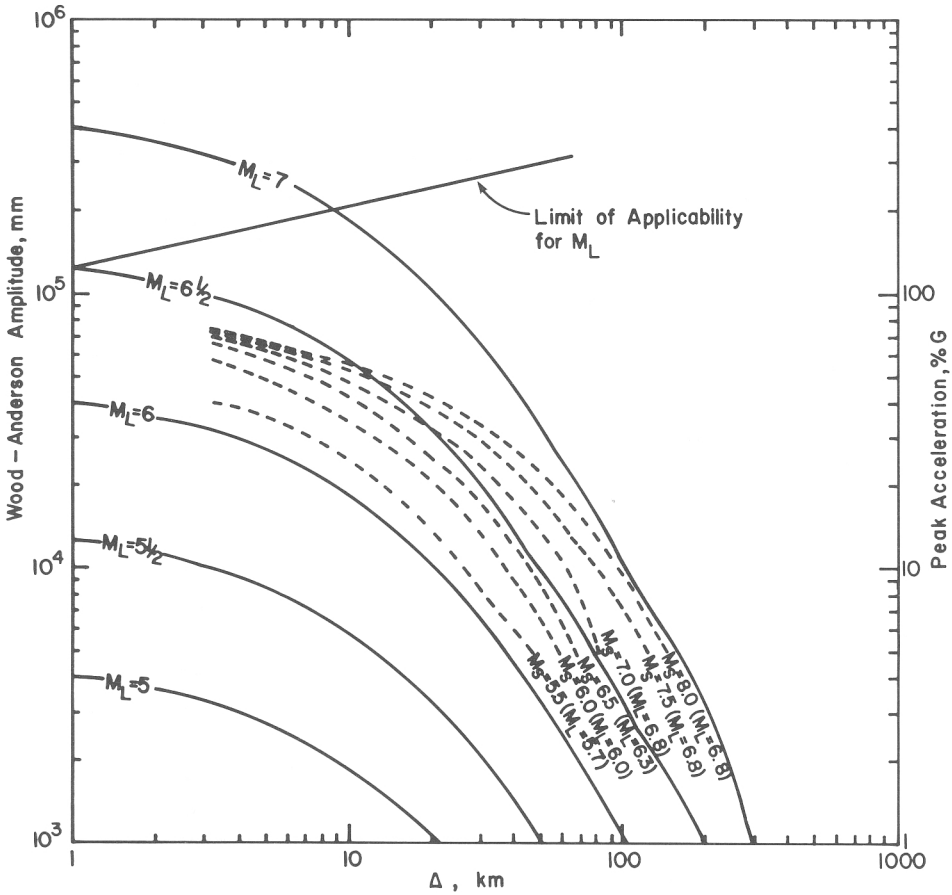

Fig. 10. Scaling of peak amplitude as measured on a Wood-Anderson torsion seismometer as a function of M_L and distance (modified distance attenuation curve assumed). Schnabel and Seed's (1973) scaling of peak acceleration with distance and magnitude (unspecified, but assumed to be M_S) is shown for comparison.

graph recording from Pacoima Dam, the station closest to the epicenter, indicated a local magnitude of 6.5. Kanamori and Jennings (1978) also calculated M_L for the 1952 Kern County earthquake and found it to be 7.2. If the Pacoima record is representative of the motions to be expected in the nearfield from an M_L 6-1/2, then what motions would we expect in the nearfield of an M_L 7.2? Taken at face value, the logarithmic scaling associated with M_L would indicate that motions in the nearfield of the Kern County earthquake were about five times those recorded at Pacoima Dam in 1971. Since the Pacoima motions were some of the most violent ever recorded, it does not seem likely that the Kern County motions were five times larger.

How large can the motion be in the nearfield? Of course, this is a question that cannot presently be answered. However, based on some rather crude, but straightforward, source models, Brune (1978) has concluded that ground velocities of order two meters per second could be expected in the nearfield of some large earthquakes. Although

Brune's estimate is defendable, based on the present knowledge of earthquake sources, there are far too few data and too much uncertainty in faulting parameters to access fully the significance of Brune's calculations. In fact, there is not sufficient control on faulting parameters to rule out the possibility of motions large enough to yield a local magnitude of 7 in the nearfield. However, building damage observed near large earthquakes has usually not been as great as engineers would have expected for such large velocities. Even this observation is complicated by the fact that the local magnitudes of most large earthquakes are lower than 7, and thus, the macroseismic effects of the nearfield motions, due to an earthquake with a local magnitude of 7, are rarely observed.

We have reached an impasse. The local magnitude scale predicts very large motions in the nearfield of earthquakes with high local magnitudes, and these large motions cannot be summarily discounted on the basis of theoretical seismological considerations. However, these large motions do not seem to be consistent with the observed damage of large earthquakes. Due to a lack of data, the problem of the sizes of motions in the nearfield of a larger earthquake (in the sense of M_L) is unresolved. However, based on observations of macroseismic effects, it is our opinion that the M_L scale is inappropriate to scale the nearfield motions of earthquakes with M_L greater than 6-1/2. In addition, it seems unlikely that future nearfield recordings will yield an M_L greater than 6-3/4. Because of our poor understanding of very nearfield motions from large earthquakes, we have included a limit on the range of applicability for the curves shown in Figure 10.

2.3. Estimation of local magnitude

We have discussed how the overall size of an earthquake can be estimated through the use of seismic moment. We also discussed how the local magnitude scale can be used to scale the sizes of strong ground motion. Furthermore, we demonstrated that there is a general relationship between local magnitude and seismic moment. In this section, we refine the relationship between local magnitude and seismic moment by including considerations of tectonic setting and local site conditions.

Up to now, we have stressed the relationship between M_L and the earthquake source. We assumed that distance was the only parameter that needs to be considered other than the source characteristics. However, it is clear that the nature of the observed motions also depends on the velocity structure of the medium through which the waves travel. The effects of the travel path are so complex and varied, that a complete parameterization of the problem appears impossible. It is possible, however, to parameterize at least a small portion of this problem in a rather simple way. The conditions of the local soil can be characterized by estimating the stiffness. In this study, we will use the following convention: 0 represents soft alluvium deposits, 2 represents basement or crystalline rocks, and 1 represents an intermediate condition such as sedimentary rocks. This particular soil classification is explained more fully by Trifunac and Brady (1975). Although more elaborate soil classifications have been

devised, it seems rather pointless to give a detailed parameterization of the soils when so many other physical parameters are ignored. As could be expected, the great variation in other physical parameters tends to obscure the relationship between the amplitudes of ground motions and the local soil conditions. In general, it appears that soft soils produce larger ground motions. Trifunac (1976) has studied this in some detail and he found that this effect is frequency dependent. He found the weakest correlation existed for peak accelerations, while the strongest correlation existed for peak displacement. Most of the data used in Trifunac's (1976) study was recorded during the 1971 San Fernando earthquake. Liu and Heaton (1984) studied the strong-motion waveforms of this event and concluded that the excitation of surface waves in large sedimentary basins is the principle reason why soft sites recorded relatively larger long-period motions than bedrock sites. Trifunac's study of peak velocity suggests the following site correction for the local magnitude scale; add 0.15 for sites designated 0, do not correct sites which are designated 1, subtract 0.15 for sites designated 2.

It is interesting to note that most accelerograms (approximately 2/3) have been recorded on sites which are classified as soft alluvium. We consider our uncorrected-sites to be intermediate sites and, since Kanamori and Jennings (1978) did not apply site correction factors in their computation of M_L, their values are systematically higher (by about 0.1 unit) than those which would be computed using a site correction factor.

Earlier, we pointed out that there is both theoretical and empirical justification for a saturation of the local magnitude scale for earthquakes beyond a certain size. The level at which the local magnitude scale saturates is an issue of central importance in the estimation of strong ground motions. In Figure 4, we showed the empirical relationship between M_s and M_L which was derived from the data sets of Gutenberg and Richter (1956) and Kanamori and Jennings (1978). A local magnitude of 7-1/4 (Kern County earthquake) is presently the highest M_L recorded. If we assume that Kern County is fairly typical of intraplate (high stress drop) earthquakes, and if we account for the fact that 7-1/4 represents values measured on soft soil sites, then we would recommend a saturation value of 7.1 for intraplate earthquakes with sites having intermediate site conditions.

In Appendix I we investigate hypothetical fault models to deduce that the saturation level of different magnitude scales should be proportional to Log $\Delta\sigma$ (Equation (I.32)). This relationship is in agreement with the notion that the average dislocation velocity is proportional to stress drop. If ground velocity is linearly related to dislocation velocities, then we expect the saturation of M_L to depend on Log $\Delta\sigma$. Thus if we assume that $M_L = 7.1$ represents the average local magnitude saturation of intraplate earthquakes with stress drops of about 60 bars, one would expect interplate earthquakes with 30 bar stress drops to have an average local magnitude saturation level of about 6.8, and the average local magnitude saturation level of shallow subduction-zone events would be about 6.5 since their average stress drop appears to be about 15 bars. These values assume intermediate site conditions.

In Appendix II, we compare strong ground motions recorded in Japan with those recorded in the western U.S. We find that the distribution of available Japanese records

with respect to earthquake magnitude and site distance is markedly different from the distribution of U.S. records. In contrast to U.S. records, there are few Japanese records available at small distances from moderate to large earthquakes. There are, however, many recordings of large off-shore Japanese subduction zone earthquakes that are taken at large distances. Despite the difference in distribution of available strong motion records and the obvious difference in tectonic setting, we find that when ground motions observed at comparable site distances and earthquake magnitudes are compared, Japanese and U.S. motions are remarkably similar. Calculation of the local magnitudes of large Japanese subduction zone earthquakes indicates a local magnitude saturation level of about 7-1/4. This value is comparable to the value we deem appropriate for intraplate crustal events. This seems to contradict our speculation that subduction zone earthquakes should exhibit a relatively lower magnitude saturation level due to their lower average stress drops. However, average stress drop is not the only source parameter that is significantly different when comparing large crustal and subduction zone earthquakes. Subduction zone earthquakes may have both large fault lengths and widths, whereas crustal earthquakes may have large fault lengths, but the fault widths are limited. In general, a recording site is most affected by that part of the rupture that is closest to it. Thus, we generally expect long, narrow faults to have relatively less area of faulting nearby to any site than does a nearly square fault. Also, square faults produce larger dislocations than long, narrow faults of equal area and stress drop (Equation (11)). For these reasons, we expect subduction zone events, with

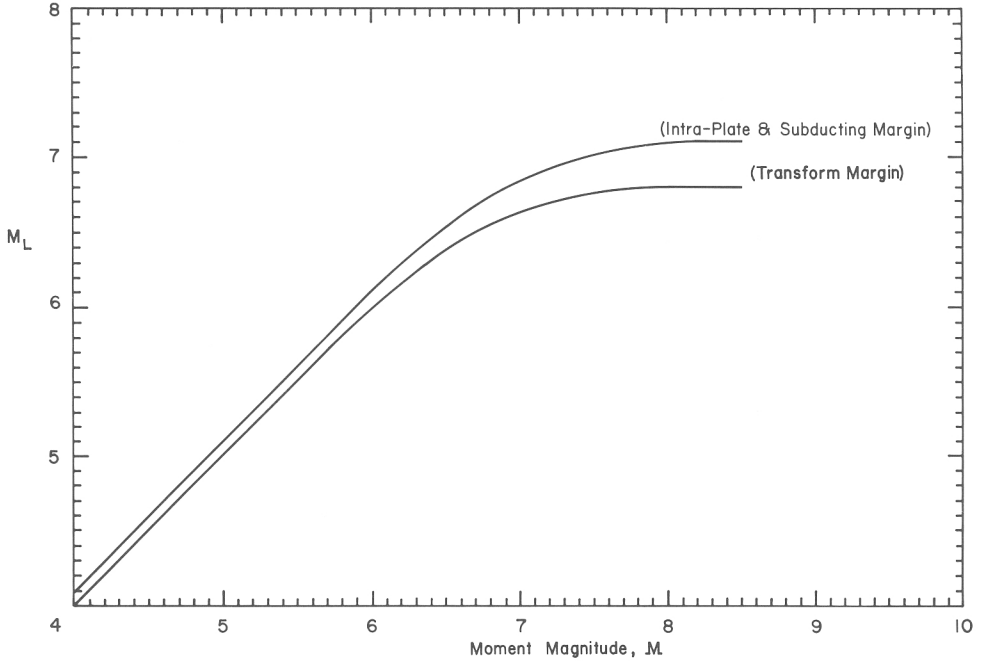

Fig. 11. Assumed average relationship between local magnitude and moment magnitude for three different tectonic regimes.

their relatively large fault widths, to have higher levels of local magnitude saturation than events with long, narrow faults and equal stress drops. Exactly how stress drop and fault aspect ratio trade off is not presently understood. However, evidence presented in Appendix II, supports the local magnitude saturation of about 7-1/4 for subduction zone events. As we pointed out in the last section, there are reasons to believe that the local magnitude distance attenuation curve may not be appropriate for very large earthquakes and small source distances. We can anticipate that fault aspect ratio will be an important parameter in the solution of this problem.

In this study, we will assume that the basic relationship between moment magnitude and local magnitude is the one that is shown in Figure 11. It is derived from empirical data, Equation (I.32), and the arguments just given. It is important to recognize that both our data and our source theory are quite limited. Thus, this relationship must be considered to be a crude hypothesis that includes stress drop, a parameter which the study of simple source models indicates is of fundamental importance in the scaling of seismic radiation. It is also important to recognize that our understanding of the stress drop of earthquakes is fairly limited. Stress drop cannot be measured directly and must instead be inferred from estimates of fault slip and fault dimensions. Kanamori (1980) has summarized many of the important studies of the state of stress in the earth's lithosphere. Figure 12 is taken from his paper and shows the calculated stress drops of

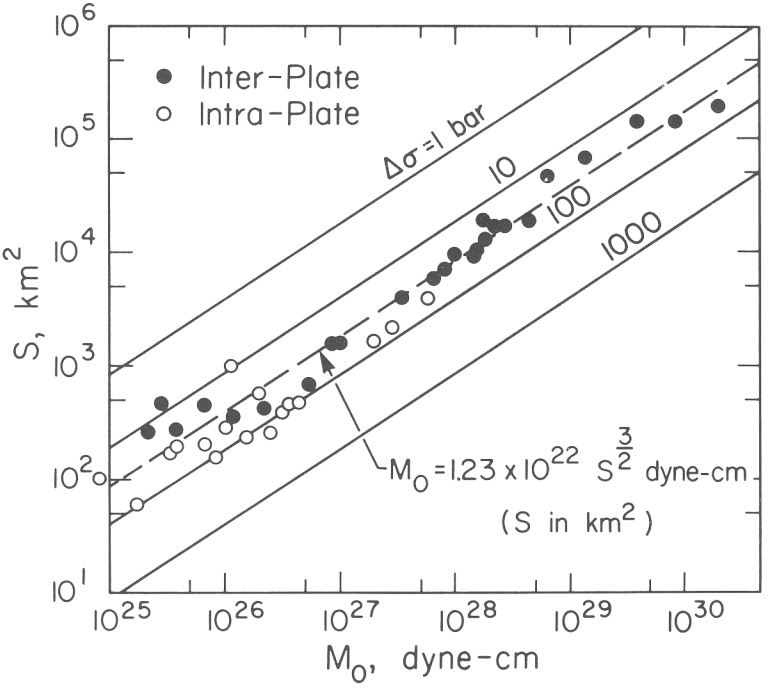

Fig. 12. Relationship between fault area and seismic moment. The solid lines denote constant stress drops and the dashed line ($M_0 = 1.23 \times 10^{22}\, S^{3/2}$ dyne-cm; S in km^2) signifies a stress drop of about 30 bars. Solid points denote interplate earthquakes and open circle denote intraplate earthquakes. This figure is taken from Kanamori (1980) and is used with permission from the author.

well-studied earthquakes as a function of earthquake size. It is clear from Figure 12 that stress drop is not a parameter which can be accurately predicted. However, it is of such physical importance that an understanding of the strong ground motions would be very difficult without it. Thus, the relationships given in Figure 11 are our attempt to include stress drop in an average way.

3. Seismic Design Guidelines

3.1. Guidelines for estimating the motions from small and moderate earthquakes

In the previous sections we concentrated on understanding the sizes of earthquakes, the scaling of strong ground motion, and the relationships between earthquake size and the amplitude of strong ground motion. In this section we demonstrate a technique for estimating ground motion time histories based on estimates of fault dimensions and tectonic setting. As was stated in the introduction, we modify and expand a technique that is described by Guzman and Jennings (1976). The basic idea is to find records from sites with settings similar to those for the area to be studied. The local magnitude scale is used to scale these records with respect to distance, site condition, and earthquake size. Because of the many problems that are associated with such scaling, it is important that we use records that require minimal scaling. Since the data set is very limited, this is not always easy. In particular, there are no strong motion records of giant ($M > 8\text{-}1/2$) earthquakes, and for these earthquakes, the procedure described in this section is not recommended.

From all we have said in the preceding section, it should be clear that we feel that merely specifying a surface wave magnitude and a distance is insufficient input to derive the ground motions expected at a particular site. Given no constraints, what would be the best way to estimate the future motions at a site? The most obvious answer to this problem would be to have a collection of all the ground motions experienced by that site over the last several thousand years. We could then forget about the difficulties associated with understanding the physics of what controls the ground motions. Although this solution is unattainable, it gives the basic philosophy for the procedure we will describe. By collecting records from sites with geologic conditions that are similar to the study site, we can incorporate important physical parameters into our procedure in a very direct fashion. The major drawback in this procedure arises from the limited size of our data set. By selecting sets of the data, our ability to estimate the statistical variation within that subset becomes limited. As the data set grows, this limitation will become less important. Since the data are limited, it is possible that only a few records will be found that are appropriate for a particular site, but it is possible to include records taken under somewhat different conditions by scaling these records with the relationships that have been discussed in the preceeding sections. Obviously, it is desirable to keep such scaling to a minimum.

It is important to have access to a fairly extensive collection of strong motion data if

the procedure is to be effective. Crouse *et al.* (1981), have compiled an extensive catalogue of digitized accelerograms. Nearly 1000 accelerograms from many countries are included. This catalogue is probably unique, since it contains information about site conditions and also seismological information for causative earthquakes. Although this is the most complete strong motion catalogue that we know of, it should not be considered exhaustive. Furthermore, in our opinion, some of the parameters listed should be considered prelimary estimates. Therefore, it is recommended that a more detailed investigation of the characteristics of each earthquake be conducted for those records that are proposed for use in the design of important facilities.

The first task is to decide which records are appropriate for a particular site. The basic input parameters will be: (1) source dimensions, (2) distance from rupture, (3) tectonic setting, and (4) site conditions. Ideally, it would be nice to sidestep the problem of using magnitude as an estimate of earthquake size, and to use source dimension directly by simply finding those earthquakes with similar source dimensions. Unfortunately, the source dimensions of most earthquakes have not been well studied, and the magnitude scale must be used to estimate the overall size of an earthquake. As previously discussed, it is our opinion that moment magnitude is the best way to estimate earthquake size at this time. Given the fault dimensions, Equation (15) can be used to estimate the expected moment magnitude.

Records taken at similar distances from earthquakes of similar seismic moments can be found by studying Figure 13. In this figure, we have plotted each of the records found

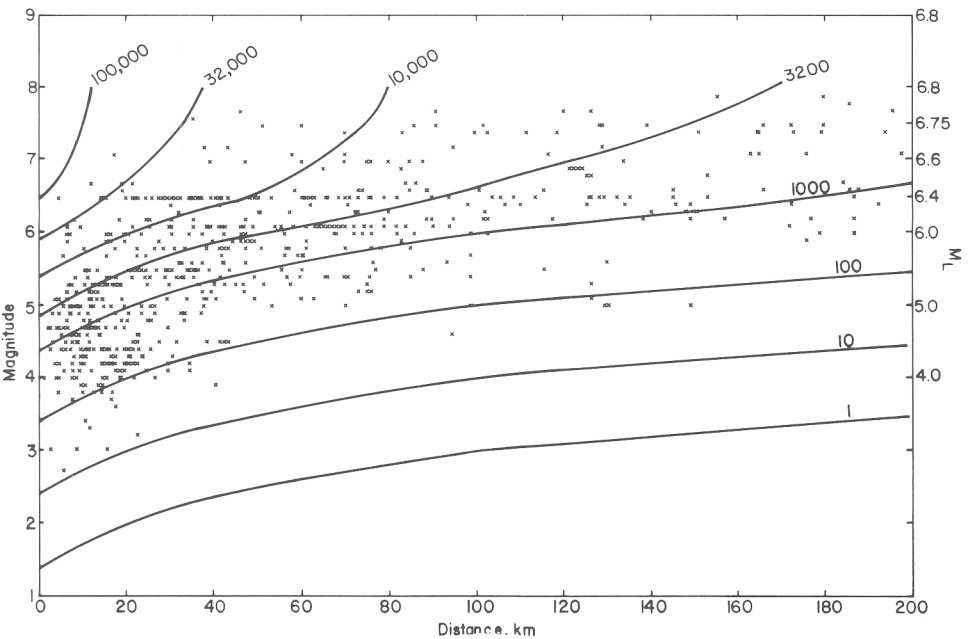

Fig. 13. Records from Crouse *et al.* (1981), catalogue plotted as a function of distance and magnitude. Contours denote theoretical lines of equal peak amplitude (milimeters) on a Wood-Anderson torsion seismometer, assuming that the vertical scale is approximately equal to moment magnitude and the stress drop is 30 bars.

in the Crouse *et al.* (1981), catalogue as a function of magnitude and distance. Although the magnitudes plotted are not moment magnitude, some care was taken to choose the magnitude value that was not affected by the saturation phenomenon which was described earlier. Notice that all of our records are for earthquakes with moment magnitudes of less than 8.

Also shown in Figure 13 are contours of equal local magnitude scaling, that is, equal peak amplitude as measured on a Wood- Anderson seismometer. These contours are for an average stress drop of 30 bars, and can be derived directly from our hypothesized relationship between local magnitude and moment magnitude, which is shown in Figure 11, and from the modified version of Richter's original distance attenuation law, which is shown in Figure 8. Records that fall along the same contour should have approximately equal peak spectral velocity.

We will now describe the procedure that, in our opinion, is appropriate for obtaining the ground motions which can be expected at a particular site.

(1) Characterize the source type and tectonic setting.
(2) Determine the dimensions of the expected rupture surface, and then calculate a moment magnitude using Equation (15).
(3) Determine the closest distance from the site to the rupture surface.
(4) Determine the site conditions (soft, intermediate, and hard) (Trifunac and Brady, 1976).
(5) Determine M_L (site) for postulated earthquake by using Steps 1 and 2 and Figure 11.
(6) Determine site correction factor C_s, where $C_s = 0.15$ for soft, 0 for intermediate, and -0.15 for hard.
(7) Determine distance correction A_0 (site) using Figure 8.
(8) Compute expected amplitude on a Wood-Anderson seismometer using the formula,

$$A_{(\text{site})} = a_0 10^{(M_L \to C_s)}. \tag{19}$$

(9) Search the Crouse *et al.* (1981), catalogue for records taken at similar distances and with similar magnitudes and tectonic settings. Choose as many records as possible. Index the records $i = 1, \ldots n$.
(10) For each earthquake, determine a moment magnitude. Use either published estimates of seismic moment or convert other magnitudes to moment magnitude using Figure 6.
(11) For each record, determine an M_L^i using the estimated moment magnitude of the earthquake and Figure 11.
(12) Determine site correction factor C_s^i for each record.
(13) Determine distance correction factor A_0^i for each record; use figure 8.
(14) Compute expected amplitude on a Wood-Anderson seismometer for each record using the formula,

$$A^i = A_0^i \, 10^{(M_1^i + C_1^i)}. \tag{20}$$

(15) Multiply the i^{th} record by the scaling factor s_i, where

$$S_i = \frac{A_{(\text{site})}}{A^i}. \tag{21}$$

The end result of this process is a suite of n records that should be representative of the types of motion that could be expected at the study site. Since the scaling process is not well understood, it is desirable to use records that require as little scaling as is possible. As Guzman and Jennings (1976) stated, 'the final product of the scaling procedure is only dependent on relative values, not on the absolute values of acceleration' (amplitude on a Wood-Anderson seismometer for this procedure). This means that the scaling factors depend primarily on the shapes and relative amplitudes of the attenuation curves for different magnitudes.

We now give an example of how this procedure can be used to obtain a free-field design spectrum. In this example, we assume a site that lies at a distance of 50 km from a strike-slip fault that has dimensions appropriate for producing an earthquake with a moment magnitude of 6-1/2. We will further assume that the study site is of intermediate hardness. Figure 13 shows that there are a number of records that could be included in our suite of records. We use the fifteen records (thirteen western United States and two Japanese) listed in Table II as our set of analogous records. We have also used the steps outlined previously to compute a scale factor for each record. Notice that only records with scaling factors of less than 2 have been chosen. Also listed are both the scaled and unscaled average peak horizontal ground velocities. If the unscaled velocities are averaged over all records, then we obtain a value of 14.3 centimeters per second (cm sec^{-1}) with a standard deviation of 8.5 cm sec^{-1}. The scaled velocities, however, scatter less and yield an average value of 17.9 cm sec^{-1} with a standard deviation of 9 cm sec^{-1}. The highest scaled velocity is 35.1 cm sec^{-1}, and the lowest is 3.6 cm sec^{-1}. Although this variation may seem large, it reflects the true uncertainty in the answer given our present level of understanding of earthquake motions.

It is worth noting that both the highest and lowest scaled average peak velocities in Table II were produced by a single earthquake, the 1979 Imperial Valley earthquake. The difference in peak velocities between stations at Delta and Plaster City is nearly an order of magnitude. Yet both stations are located within the Imperial Valley at roughly comparable distances from the earthquake rupture. Although there are undoubtedly good physical explanations for this difference, it probably would have been quite difficult to predict this result. It is also worth noting that the third highest and second lowest velocities are from two records which were also produced under nearly identical circumstances. That is, records #4 and #8 are both from the station at El Centro, California, and were produced by M_s 6-1/2 earthquakes on the Coyote Creek fault. In fact, the two earthquakes (1942 Borrego Valley and 1968 Borrego Mountain) occurred very close to one another. Nevertheless, the El Centro records from the closer 1942 earthquake are much smaller than the records from the 1968 earthquake. A close

TABLE II

No.	Earthquake	Station	Magnitude M_w (if available)	Center of energy distance (km)	Soil type	Calculated M_L	$-\text{Log}\, A_0$	C_s	A_i (m)	Scale factor	Avg. peak horizontal velocity (cm sec^{-1})	Avg. scaled peak velocity (cm sec^{-1})
1	3/11/33 Long Beach	Vernon CMD Bldg.	6.3	36	0	6.23	2.28	+0.15	12.59	0.87	23.	20.
2	3/11/33 Long Beach	L.A. Subway Term.	6.3	42	0	6.23	2.38	+0.15	10.0	1.10	20.5	22.6
3	12/30/34 L. California	El Centro	6.5	61	0	6.38	2.61	+0.15	8.32	1.32	16.0	21.1
4	10/21/42 Borrego Valley	El Centro	6.5	46	0	6.38	2.44	+0.15	12.3	0.89	6.2	5.5
5	12/21/54 Eureka	Ferndale City Hall	6.5	40	1	6.38	2.35	0	10.72	1.02	31.	31.6
6	4/20/65 Japan	Site #CB005	6.1	50	0	6.08	2.43	+0.15	6.31	1.74	9.6	16.7
7	4/20/65 Japan	Site #CB002	6.1	45	0	6.08	2.49	+0.15	5.50	1.99	7.8	15.5
8	4/ 9/68 Borrego Mtn.	El Centro	6.6	65	0	6.45	2.65	+0.15	8.91	1.23	20.2	24.8
9	10/15/79 Imperial Valley	Cerro Prieto	6.4	39	2	6.3	2.33	−0.15	6.61	1.66	15.	24.9
10	10/15/79 Imperial Valley	Delta	6.4	50	0	6.3	2.49	+0.15	9.12	1.2	29.2	35.1
11	10/15/79 Imperial Valley	Victoria	6.4	60	0	6.3	2.6	+0.15	7.08	1.55	10.2	15.8
12	10/15/79 Imperial Valley	Calipatria	6.4	41	0	6.3	2.37	+0.15	12.02	0.91	13.7	12.4
13	10/15/79 Imperial Valley	Superstition	6.4	42	0	6.3	2.39	+0.15	11.48	0.95	6.9	6.6
14	10/15/79 Imperial Valley	Plaster City	6.4	38	0	6.3	2.32	+0.15	13.49	0.81	4.5	3.6
15	10/15/79 Imperial Valley	Niland	6.4	51	0	6.3	2.5	+0.15	8.91	1.23	10.1	12.4
	Test Case		6.5	50	0	6.38	2.49	+0.15	10.96		14.92 ± 8.0	17.91 ± 8.9

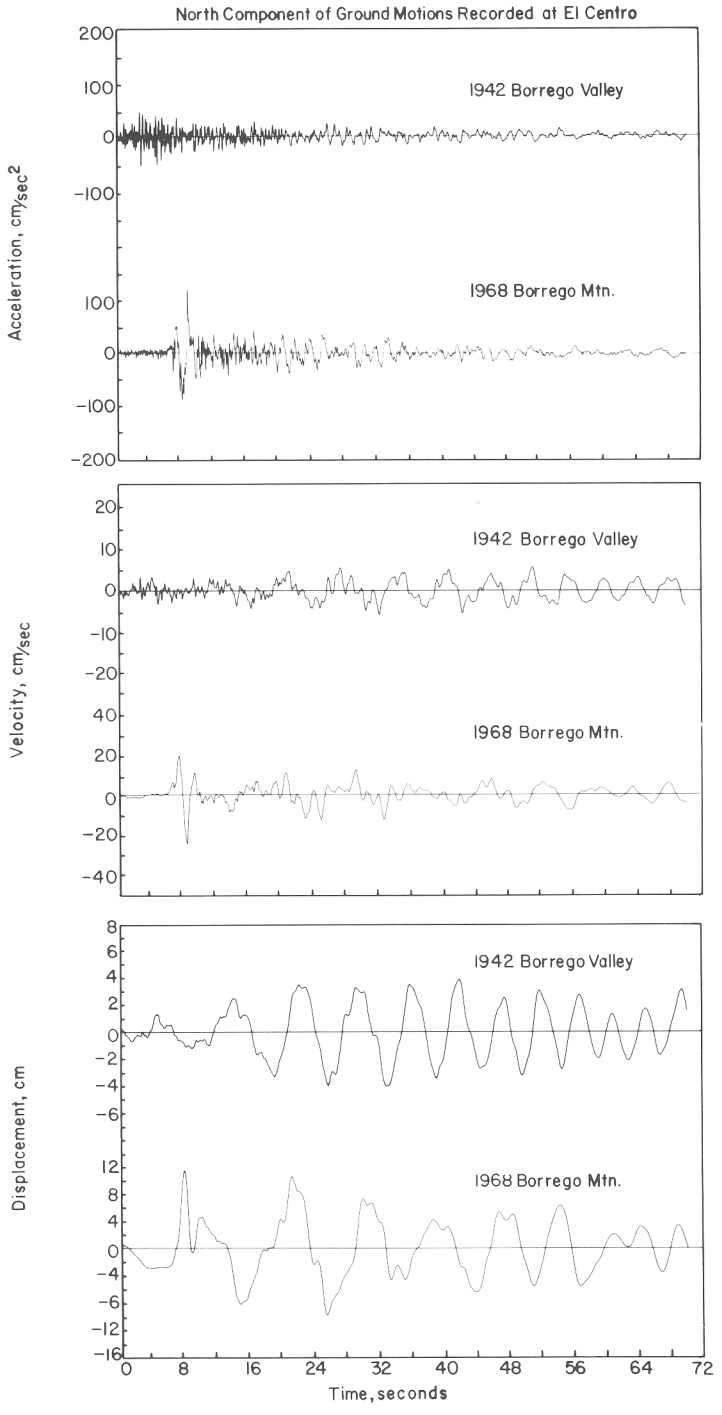

Fig. 14. North component of ground motion for two M 6-1/2 Borrego, California earthquakes as recorded at El Centro. Note that the 1942 records are plotted on an amplitude scale half as large as that used to plot the 1968 records.

inspection of the motions produced at El Centro by those earthquakes reveals striking similarities and differences. The long-period surface wave parts of the records are very similar and yet, the higher-frequency acceleration time histories are very different. This can be seen in Figure 14 that shows the processed records of the north component of motion recorded at El Centro for the 1942 and 1968 earthquakes. The exact causes for the differences between the records in Figure 14 are a matter of future study. However, there is presently an important lesson to be learned from these records. Although we may approximately scale for site effects, source dimensions, travel path, and tectonic setting, there are also very important indeterminate parameters associated with the earthquake source.

In Figure 15, we show the scaled response spectra (3% damping) for the horizontal components of records in our suite. In general, the scatter is about an order of magnitude. Furthermore, records that have the largest values at high frequencies may have relatively small values at low frequencies. Although this large scatter may not

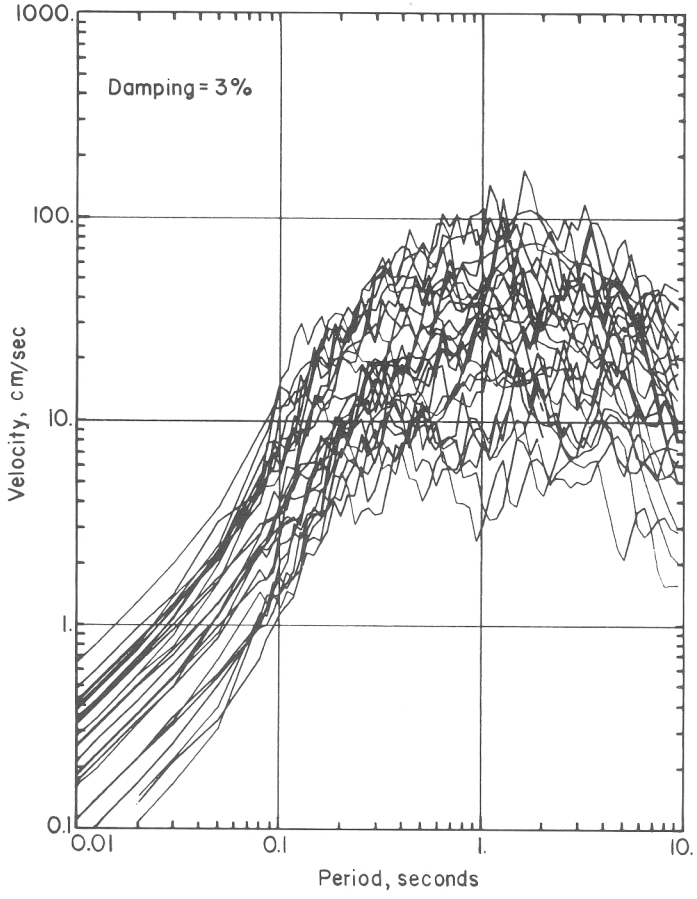

Fig. 15. Response spectra (3% damped) for horizontal components of 15 records from strike-slip earthquakes which are scaled to a distance of 50 km and a magnitude of 6-1/2.

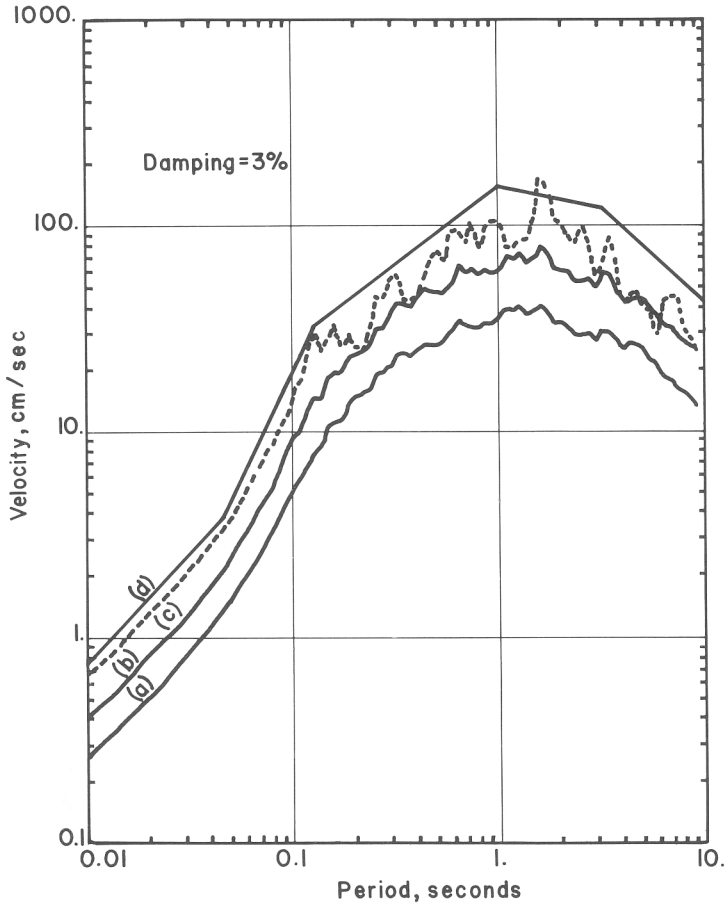

Fig. 16. (a) Average spectrum, (b) average plus one standard deviation spectrum, (c) spectrum of the largest single record, (d) spectrum which envelops all others; based on spectra shown in Figure 17.

seem very satisfactory, it represents our ability to parameterize strong ground motion in terms of magnitude, distance, soil condition, and fault type. We show an example of how the free-field design spectrum for a M 6-1/2 strike-slip earthquake at a distance of 50 km can be chosen in Figure 16. The average spectrum, the average plus one standard deviation spectrum, the spectrum of the single largest record, and the spectrum which envelops all others are shown. The suite of spectra shown in Figure 15 forms the basis for these choices of design spectra.

4. Conclusions

We have presented a procedure for estimating ground motions using simple scaling of existing recorded ground motions. The scaling procedure incorporates fundamental seismological concepts regarding the sizes of earthquakes and the saturation of

different magnitude scales. We have seen that considerable ambiguity may be present when the term earthquake 'magnitude' is loosely defined. We choose to define earthquake size in terms of seismic moment. We have parameterized strong ground motions using M_L scale. We suggest that saturation of the local magnitude scale may vary systematically with average earthquake stress drop which may in turn vary systematically with tectonic setting. Although subduction zones may produce the largest earthquakes, they do not necessarily produce the most intense ground shaking. Furthermore, relatively rare intraplate earthquakes may produce relatively severe ground motions.

The procedure we have presented conserves a meaningful measure of the uncertainty inherent when predicting ground motions from a simple parameterization of earthquake size and station distance. In an example, we showed that although the scatter may be as much as an order of magnitude, it would be extremely difficult to reduce that scatter by a better parameterization of the earthquake source or the recording site.

Appendix I: Spectral Scaling Relations

In this appendix we discuss the relationship between earthquake magnitude and rupture parameters for several simple models of the earthquake source. These relationships are derived from estimates of the Fourier amplitude spectra of seismic energy produced by our simple source models.

We begin with some simple observations about the way magnitude is related to Fourier spectral amplitude. Let us define a hypothetical magnitude scale M_T that is the logarithm of the peak amplitude of a specified wavetrain on a seismogram produced by a specified seismometer. Seismogram wavetrains may have a wide variety of characteristics, depending upon the nature of the input ground motion and the response of the seismometer. In general, we can break the problem into the following four categories.

(i) A seismogram wavetrain consists of a near monochromatic waveform. Such waveforms are often produced by narrow-band seismometers or by wavetrains that are well-dispersed by wave propagation. In this case, we expect the peak observed seismogram amplitude to be proportional to the Fourier spectral amplitude of the signal at the dominant period of the signal. Thus, we expect that

$$M_T \sim \mathrm{Log}\left|\hat{U}\left(\frac{2\pi}{T}\right)\right|, \tag{I.1}$$

where $\hat{}$ denotes Fourier transform.

(ii) A seismogram wavetrain consists of a simple pulse that is recorded by a band-limited seismometer whose free-period is large compared to the duration of the actual ground motion. Since the duration of the signal T_L is small compared to T, we may conclude that the seismogram in this case is simply the impulse response of the instrument. Hence

$$M_T \sim \mathrm{Log}\left|\hat{U}\left(\frac{2\pi}{T \to \infty}\right)\right| \sim \mathrm{Log}\,\hat{U}\left|\left(\frac{2\pi}{T}\right)\right|. \tag{I.2}$$

(iii) A seismogram wavetrain consists of a simple pulse that is produced by a simple pulse in ground displacement as recorded on a broad-band seismometer. This case may arise when observing body waves on simple damped harmonic oscillators whose period T is longer than the signal duration T_L. In this case, the peak seismogram amplitude is proportional to the area of the pulse divided by its pulse width and thus,

$$M_T \sim \text{Log}\left|\frac{\hat{U}\left(\frac{2\pi}{T \to \infty}\right)}{T_L}\right| \sim \text{Log}\left|\frac{\hat{U}\left(\frac{2\pi}{T}\right)}{T_L}\right|. \tag{I.3}$$

(iv) A seismogram wavetrain consists of a complex collection of randomly spaced pulses. This case may arise when observing body waves on a simple damped harmonic oscillator whose period T is short when compared with the signal duration T_L. In this case, the Fourier spectra of the individual pulses can be summed with random phase in order to produce the total seismogram. The amplitude spectrum of the sum of m impulses of random phase is simply proportional $\sqrt{\text{m}}$. Thus, the amplitude spectrum of the ground motion is proportional to the square root of the signal duration. Thus,

$$M_T \sim \text{Log}\left|\frac{\hat{U}\left(\frac{2\pi}{T}\right)}{\sqrt{T_L}}\right|. \tag{I.4}$$

Actually, real seismograms do not usually fit completely into any of these categories. However, it is clear from the preceding discussion that a general definition of M_T is given by the following:

$$M_T \sim \text{Log}\left|\hat{U}\left(\frac{2\pi}{T}\right)\right| - \xi \,\text{Log}\, T_L, \tag{I.5}$$

where $0 < \xi < 1$ and ξ depends upon the type of seismometer and wavetrain that is observed.

We can now demonstrate how our generalized magnitude scale M_T behaves as a function of rupture parameters for several simple source models. First we investigate a model that was initially introduced by Haskell (1964). This model assumes that faulting occurs uniformly on a rectangular surface. A finite, planar fault in a homogeneous whole-space is assumed. The receiver is assumed to be at distances that are large when compared to the fault dimensions. Rupture initiates along a line, and the linear rupture front proceeds along the fault length at constant velocity. The dislocation time history for every point on the fault is assumed to be a linear ramp in time. A sketch of this fault model is found in Figure 17. Although this is a very simple fault model, it does allow us to demonstrate phenomena that help explain the differences between various magnitude scales. The following discussion was developed by Kanamori and Anderson (1975) and later extended by Geller (1976) and Noguchi and Abe (1977).

Let us investigate the nature of motions which are produced by the model just described.

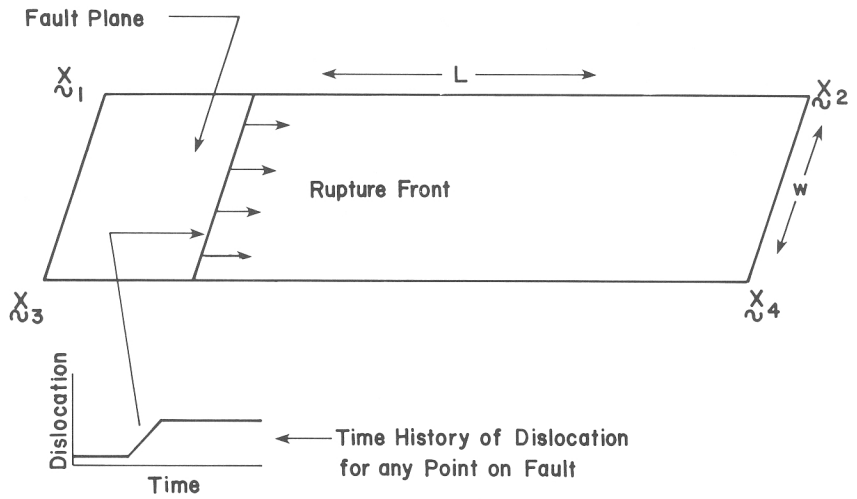

Fig. 17. Schematic of Haskell-type fault model.

Define a boxcar function, $B(t/\tau)$, as follows:

$$B(t/\tau) \equiv \begin{cases} 0, & t/\tau > 0 \\ 1, & 0 < t/\tau < 1 \\ 0, & t/\tau > 1. \end{cases} \tag{I.6}$$

Furthermore, define

$$T_{ij} = T_i - T_j,$$

where T_i and T_j are the arrival times of energy from the i_{th} and j_{th} corners of the fault, respectively. It can be shown that the displacement history at the receiver can be approximated by the following relationship:

$$U(t) \sim M_0 B(t/T_{13}) * B(t/T_{12}) * B(T/\tau), \tag{I.7}$$

where M_0 is the seismic moment, τ is the duration of the dislocation time history and * denotes convolution. Let M_T be the magnitude scale that is defined in Equation (I.5) and, for simplicity, let us assume that $\xi = 0$. Taking the Fourier transform of (I.7), we obtain

$$M_T \sim \operatorname{Log} M_0 \left| \frac{\operatorname{Sin}\left(\frac{\pi T_{13}}{T}\right)}{\frac{\pi T_{13}}{T}} \right| \left| \frac{\operatorname{Sin}\left(\frac{\pi T_{12}}{T}\right)}{\frac{\pi T_{12}}{T}} \right| \left| \frac{\operatorname{Sin}\left(\frac{\pi \tau}{T}\right)}{\frac{\pi \tau}{T}} \right|. \tag{I.8}$$

We now postulate the following similarity conditions:

$$w \sim \alpha L, \tag{I.9}$$

$$\dot{D} \sim \Delta\sigma, \tag{I.10}$$

$$\frac{D}{\alpha L} \sim \Delta\sigma, \tag{I.11}$$

where w is fault width, and L is fault length, and α is a constant which gives the aspect ratio of the rupture surface. Relationship (I.10) is the only one that we have not yet introduced. This relationship was introduced by Brune (1970) and it states that the dislocation velocity is proportional to the stress drop (provided certain dynamic conditions are met). Since $D(t)$ is assumed to be a ramp,

$$\tau = \frac{D}{\dot{D}} \tag{I.12}$$

and from (I.10), (I.11), and (I.12), we conclude that

$$\tau \sim L\alpha \sim M_0^{1/3}\, \Delta\sigma^{-1/3}\, \alpha^{1/3}. \tag{I.13}$$

From the definition of T_{ij}, it is also clear that

$$T_{13} \sim w \sim L\alpha \sim M_0^{1/3}\, \Delta\sigma^{-1/3}\, \alpha^{1/3}, \tag{I.14}$$

and

$$T_{12} \sim L \sim M_0^{1/3}\, \Delta\sigma^{-1/3}\, \alpha^{-2/3}. \tag{I.15}$$

we can now derive the relationship between M_T and moment magnitude as L increases. We approximate the function $(\sin x)/x$ by its extremal asymptotes ($= 1$ if $x \to 0$; $= 1/x$ if $x \to \infty$). We separate the problem in the following cases.

(i) L very small and then τ, T_{13}, and T_{12} are small compared to T/π and (I.8) reduces to

$$M_T \sim \operatorname{Log} M_0 \sim \tfrac{3}{2} M. \tag{I.16}$$

(ii) L becomes large enough so that $\tau < T_{13} < T/\pi < T_{12}$ and then

$$\begin{aligned} M_T &\sim \operatorname{Log}\left(M_0 \frac{1}{T_{12}}\right) \sim \operatorname{Log}\left(M_0^{2/3}\, \Delta\sigma^{1/3}\, \alpha^{2/3}\right) \\ &\sim M + \tfrac{1}{3}\operatorname{Log} \Delta\sigma + \tfrac{2}{3}\operatorname{Log}\alpha. \end{aligned} \tag{I.17}$$

(iii) L larger yet, $\tau < T/\pi < T_{13} < T_{12}$ and

$$\begin{aligned} M_T &\sim \operatorname{Log}\left(\frac{M_0}{T_{12} T_{13}}\right) \sim \operatorname{Log}\left(M_0^{1/3}\, \Delta\sigma^{2/3}\, \alpha^{1/3}\right) \\ &\sim \tfrac{1}{2} M + \tfrac{2}{3} \operatorname{Log} \Delta\sigma + \tfrac{1}{3} \operatorname{Log}\alpha. \end{aligned} \tag{I.18}$$

(iv) Finally, for L very large, $T/\pi < \tau < T_{13} < T_{12}$ and

$$M_T \sim \operatorname{Log}\left(\frac{M_0}{\tau T_{13} T_{12}}\right) \sim \operatorname{Log} \Delta\sigma. \tag{I.19}$$

In Figure 18, we sketch the approximate relationship between moment magnitude and magnitude M_T based on spectral amplitude at a certain period. Although this is a very simple source model, it does illustrate several features that should be observed for actual earthquakes. For instance, a comparison of M_s vs M in Figure 5 shows a similar

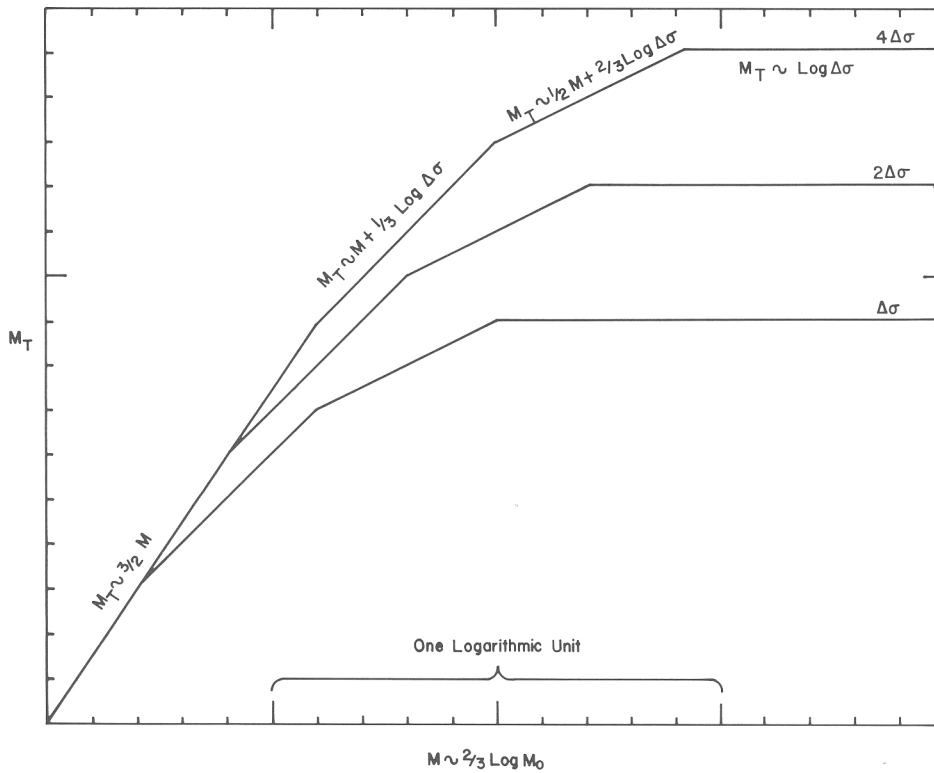

Fig. 18. Schematic showing the way in which any band-limited magnitude scale depends upon moment magnitude assuming a simple Haskell-type fault model and three different values of stress drop. The shapes of the curves are given by Equations (I.16) through (I.19).

form to the one that we just derived. We note that this model predicts that the effect of stress drop becomes important only as our hypothetical magnitude scale begins to saturate. We also note that both the stress drop and the fault aspect ratio are relatively important parameters in determining the period at which saturation occurs.

Unfortunately, the model of source rupture just presented is still far too simple in several important aspects. For instance, it has become clear that earthquake rupture is not uniform over a fault surface. In the homogeneous faulting model just presented, high-frequency radiation appears only at the beginning and end of the observed motion. Real seismograms, however, are usually characterized by high-frequency arrivals that are randomly spaced throughout the entire duration of ground motion. At small length and time scales it may be more appropriate to characterize variations in the rupture process with statistical parameters (Haskell, 1966; Aki, 1968; Andrews, 1980).

We now introduce a new spectral scaling law that relates source dimensions to spectral characteristics of U. Although this law is more general than that given in Equation (I.7), it is rather ad hoc. It also shares features of other source models in which the rupture time and dislocation amplitude are allowed to have a specified degree of

random variation on the fault surface. Assume that

$$\hat{U}\left(\frac{2\pi}{T}\right) \sim M_0 \left| \frac{\mathrm{Sin}\left(\frac{\pi t_1}{T}\right)}{\frac{\pi T_1}{T}} \right|^{v_1} \left| \frac{\mathrm{Sin}\left(\frac{\pi T_2}{T}\right)}{\frac{\pi T_2}{T}} \right|^{v_2} \left| \frac{\mathrm{Sin}\left(\frac{\pi T_3}{T}\right)}{\frac{\pi T_3}{T}} \right|^{v_3}, \tag{I.20}$$

As before, assume the following similarity conditions.

$$w = \alpha L, \tag{I.21}$$

$$\bar{D} \sim \Delta\sigma w \sim \Delta\sigma\alpha L, \tag{I.22}$$

where $\bar{\ }$ denotes the averge over the fault surface. Further assume that

$$\bar{D} \sim \Delta\sigma, \tag{I.23}$$

then

$$M_0 \sim \bar{D} w L \sim \Delta\sigma\alpha^2 L^3. \tag{I.24}$$

We further assume that

$$T_1 \sim T_L \sim L \sim M_0^{1/3} \Delta\sigma^{-1/3} \alpha^{-2/3}, \tag{I.25}$$

$$T_2 \sim w \sim M_0^{1/3} \Delta\sigma^{-1/3} \alpha^{1/3}, \tag{I.26}$$

and

$$T_3 \sim \bar{D}/\dot{\bar{D}} \sim \alpha L \sim M_0^{1/3} \Delta\sigma^{-1/3} \alpha^{1/3}. \tag{I.27}$$

T_1, T_2 and T_3 are similar to the corresponding variables defined in our earlier 'smooth' fault model, but are in general smaller quantities. This definition is motivated by Haskell's (1966) conclusion that rupture heterogeneity tends to introduce more high-frequency energy than derived from similar 'smooth' models. In our previous model, the exponents v_1, v_2 and v_3 are equal to plus one. This produces a high-frequency spectral decay rate of T^3. As random variations are added to the 'smooth' model, these exponents become less positive. When $v_1 + v_2 + v_3 < 3/2$, then the degree of heterogeneity is high enough that infinite radiated energy is produced by this spectral scaling law.

We now derive the scaling relationships between our generalized spectral magnitude M_T which is given by Equation (I.5) and the fault parameters, fault length, aspect ratio, and stress drop, assuming the scaling relationships given by Equations (I.20) through (I.27). As before, we separate the problem into 4 cases and approximate the sinc function by its extremal assymptotes. This approximation is even more appropriate in this model since random variation eliminates the spectral holes produced by the homogeneous rupture model.

(i) L very small and then T_1, T_2 and T_3 are small compared to T/π and then

$$\begin{aligned} M_T &\sim \operatorname{Log} M_0 - \xi \operatorname{Log} T_L \\ &\sim \left(1 - \frac{\xi}{3}\right) \operatorname{Log} M_0 + \frac{\xi}{3} \operatorname{Log} \Delta\sigma + \frac{2\xi}{3} \operatorname{Log} \alpha \\ &\sim \left(\frac{3 - \xi}{2}\right) M + \frac{\xi}{3} \operatorname{Log} \Delta\sigma + \frac{2\xi}{3} \operatorname{Log} \alpha . \end{aligned} \tag{I.28}$$

(ii) L becomes large enough that $T_3 < T_2 < T/\pi < T_1$, and then

$$\begin{aligned} M_T &\sim \operatorname{Log}\left(\frac{M_0}{T_1^{v_1}}\right) - \xi \operatorname{Log} T_L \\ &\sim \left(1 - \frac{\xi + v_1}{3}\right) \operatorname{Log} M_0 + \left(\frac{\xi + v_1}{3}\right) \operatorname{Log} \Delta\sigma + \left(\frac{2\xi + 2v_1}{3}\right) \operatorname{Log} \alpha \\ &\sim \left(\frac{3 - \xi - v_1}{2}\right) M + \left(\frac{\xi + v_1}{3}\right) \operatorname{Log} \Delta\sigma + \left(\frac{2\xi + 2v_1}{3}\right) \operatorname{Log} \alpha \end{aligned} \tag{I.29}$$

(iii) L larger yet, $T_3 < T/\pi < T_2 < T_1$

$$\begin{aligned} M_T &\sim \operatorname{Log}\left(\frac{M_0}{T_1^{v_1} T_2^{v_2}}\right) - \xi \operatorname{Log} T_L \\ &\sim \left(1 - \frac{\xi + v_1 + v_2}{3}\right) \operatorname{Log} M_0 + \left(\frac{\xi + v_1 + v_2}{3}\right) \operatorname{Log} \Delta\sigma + \\ &+ \left(\frac{2\xi + 2v_1 - v_2}{3}\right) \operatorname{Log} \alpha \\ &\sim \left(\frac{3 - \xi - v_1 - v_2}{2}\right) M + \left(\frac{\xi + v_1 + v_2}{3}\right) \operatorname{Log} \Delta\sigma + \\ &+ \left(\frac{2\xi + 2v_1 - v_2}{3}\right) \operatorname{Log} \alpha . \end{aligned} \tag{I.30}$$

(iv) Finally, for L very large, $T/\pi < T_3 < T_2 < T_1$ and

$$\begin{aligned} M_T &\sim \operatorname{Log}\left(\frac{M_0}{T_1^{v_1} T_2^{v_2} T_3^{v_3}}\right) - \xi \operatorname{Log} T_L \\ &\sim \left(1 - \frac{\xi + v_1 + v_2 + v_3}{3}\right) \operatorname{Log} M_0 + \left(\frac{\xi + v_1 + v_2 + v_3}{3}\right) \operatorname{Log} \Delta\sigma + \\ &+ \left(\frac{2\xi + 2v_1 - v_2 - v_3}{3}\right) \operatorname{Log} \alpha \\ &\sim \left(\frac{3 - \xi - v_1 - v_2 - v_3}{2}\right) M + \left(\frac{\xi + v_1 + v_2 + v_3}{3}\right) \operatorname{Log} \Delta\sigma + \\ &\left(\frac{2\xi + 2v_1 - v_2 - v_3}{3}\right) \operatorname{Log} \alpha . \end{aligned} \tag{I.31}$$

The value of ξ depends upon the type of seismogram used to measure peak amplitude and is, in general, also a function of T. Considering the complexity of the resulting scaling relationships, it is not too surprising to find that the various magnitude scales in use today are not interchangeable. One significant feature of this model of magnitude scaling is the fact that we can explicitly determine the relationship between stress drop and M_T simply by knowing the relationship between M_T and M. That is, in all cases (Equations (I.28) through (I.31)) we can write,

$$M_T \sim AM + (1 - \tfrac{2}{3}A)\,\mathrm{Log}\,\Delta\sigma, \tag{I.32}$$

where A is a function of fault length.

As an example of our more general scaling law, we now construct a specific model which produces a short-period spectral decay rate of T^2. For simplicity we assume that $v_1 = v_2 = v_3 = \frac{2}{3}$. We will define ξ in a way such that it is consistent with measuring both surface wave magnitude ($\xi = 0$ for all T) and a broad-band body-wave magnitude ($\xi = 1$ for $T > T_L$ and $\xi = \frac{1}{2}$ for $T < T_L$). Our solution becomes

(i) L small so that $T_3 < T_2 < T_1 < T/\pi$ and

$$M_T \sim \tfrac{3}{2}M \qquad (M_T \text{ approximates } M_s) \tag{I.33}$$

$$M_T \sim M + \tfrac{1}{3}\,\mathrm{Log}\,\Delta\sigma + \tfrac{2}{3}\,\mathrm{Log}\,\alpha \quad (M_T \text{ approximates } m_B). \tag{I.34}$$

(ii) L large enough so that $T_3 < T_2 < T/\pi < T_1$,

$$M_T \sim \tfrac{7}{6}M + \tfrac{2}{9}\,\mathrm{Log}\,\Delta\sigma + \tfrac{4}{9}\,\mathrm{Log}\,\alpha \qquad (M_T \sim M_s) \tag{I.35}$$

and

$$M_T \sim \tfrac{11}{12}M + \tfrac{7}{18}\,\mathrm{Log}\,\Delta\sigma + \tfrac{7}{9}\,\mathrm{Log}\,\alpha \quad (M_T \sim m_B). \tag{I.36}$$

(iii) L larger yet so that $T_3 < T/\pi < T_2 < T_1$

$$M_T \sim \tfrac{5}{6}M + \tfrac{4}{9}\,\mathrm{Log}\,\Delta\sigma + \tfrac{2}{9}\,\mathrm{Log}\,\alpha \qquad (M_T \sim M_s) \tag{I.37}$$

$$M_T \sim \tfrac{7}{12}M + \tfrac{11}{18}\,\mathrm{Log}\,\Delta\sigma + \tfrac{5}{9}\,\mathrm{Log}\,\alpha \quad (M_T \sim m_B). \tag{I.38}$$

(iv) Finally, L large enough that $T/\pi < T_3 < T_2 < T_1$

$$M_T \sim \tfrac{1}{2}M + \tfrac{2}{3}\,\mathrm{Log}\,\Delta\sigma \qquad (M_T \sim M_s) \tag{I.39}$$

and

$$M_T \sim \tfrac{1}{4}M + \tfrac{5}{6}\,\mathrm{Log}\,\Delta\sigma + \tfrac{1}{3}\,\mathrm{Log}\,\alpha \qquad (M_T \sim m_B). \tag{I.40}$$

By examining these hypothetical magnitude scales and source models, we have seen that the relationships between magnitude scales in use today and fault dimension and stress drop are likely to be quite complex. This is consistent with the observed complex relationships between various magnitude scales that was presented in Figure 6. The principle conclusions to be drawn from these models are: (i) magnitude scales should saturate at large fault dimension, (ii) magnitude scales based upon short-period measurements should saturate before magnitude scales based upon long-period measurements, (iii) the ratio of fault width to fault length can be an important source scaling parameter, (iv) stress drop is relatively unimportant before a magnitude scale begins to saturate, but becomes the dominant parameter after a magnitude scale saturates.

Appendix II: A Comparison of U.S. and Japanese Strong Ground Motions

The purpose of this appendix is to compare recordings of strong ground motion from Japan with those from the western U.S. To this end, we compare peak values of ground acceleration, velocity, and displacement recorded at comparable source distances and earthquake magnitudes. We also compute local magnitudes of Japanese earthquakes to study magnitude saturation for subduction zones. We have collected data from several catalogues for this comparison. Most of the digitized accelerometer data is listed in the catalogue of Crouse *et al.* (1981). Additional U.S. data are from the 1979 Imperial Valley earthquake (Brady *et al.*, 1980a) and from the 1979 Coyote Lake earthquake (Brady *et al.*, 1980b). The Japanese data is primarily from Crouse *et al.* (1981). C. B. Crouse of Ertec has graciously supplied listings of peak accelerations of unprocessed accelerograms as well. Some of the values of peak ground velocity from the 1968, M_s 7.8 Tokachi-Oki earthquake are from Inoue (1983). Finally, some unprocessed peak acceleration points from Alaska (Beavan and Jacob, 1984) are included in the Japanese data set. Unfortunately, it is beyond the scope of this study to provide a full catalogue of all recordings used for this comparison. We have, however, included a listing of all Japanese records for which we computed local magnitudes (Table III). Plots of processed records included in Table III can be found in the catalogue compiled by Mori and Crouse (1981).

The meaning of distance between the earthquake and recording site can sometimes be ambiguous. Most distances listed in Table III are either epicentral or hypocentral distances. However, when the earthquake dimension is large, some other measure of distance may be appropriate. In Figures 19 through 21, we have used the closest horizontal distance between the site and the rupture. In most instances, this means that we used the epicentral distance. In the case of the 1968, M_s 7.8 Tokachi-Oki earthquake, we computed the closest distance to the rupture surface as defined by the locations of the first several hours of aftershocks. Some of the Japanese events occur at considerable depth and in these instances, it may be more appropriate to use hypocentral distance together with a new set of distance attenuation laws. However, we found that the use of epicentral distance for earthquakes of depths up to 50 km resulted in consistent peak motions for both shallow and deeper (less than 50 km) Japanese earthquakes.

In Figures 19 through 21, we plot peak values of ground acceleration, velocity, and displacement as a function of distance for Japanese and U.S. records for selected earthquake magnitude ranges. When comparing peak values of ground motion, regardless of earthquake magnitude (Figure 19 a and b; Figure 20 a and b; Figure 21 a and b), we see that the distribution of observed Japanese ground motions is very different from the U.S. ground motions. In general, the largest ground motions have been recorded in the western U.S. at small source distances. Although there are few Japanese records of peak acceleration greater than 0.5 g, impressively large motions have been recorded at distances of 100 km and more in Japan. Taken at face value, this might suggest that ground motion attenuates less severely with distance in Japan. However, when we compare motions that were recorded at comparable earthquake

TABLE III

Earthquake		Site No.	Distance Epicentral	Distance Center of energy	Component	Log A_{wa}	$M_{L(CER)}$	$M_{L(EP)}$
2/14/56 Kashiwa Depth = 45	$M_{JMA} = 6.0$ $M_L = 6.1$	TK024	21	50	North	4.07	6.56	6.07
					East	4.09	6.56	6.09
		TK024	23	51	North	4.07	6.57	6.13
					East	4.09	6.59	6.15
4/23/62 Tokachioki Depth = 60	$M_{JMA} = 7.0$ $M_L = 7.2$	HK005	75	100	North	4.40	7.40	7.15
					East	4.49	7.49	7.2
4/30/62 Depth = 35	$M_{JMA} = 6.5$ $M_L = 6.4$	TH030	64	69	North	3.71	6.4	6.35
					East	3.73	6.42	6.37
5/8/63 Tokai Depth = 40	$M_{JMA} = 6.1$ $M_L = 6.0$	KT003	53	63	North	3.64	6.27	6.16
					East	3.62	6.25	6.14
		KT001	53	63	North	3.34	5.97	5.86
					East	3.26	5.89	5.78
8/4/63 Depth = 39	$M_{JMA} = 5.1$ $M_L = 5.8$	KT014	35	52	North	3.63	6.14	5.9
					East	3.39	5.9	5.66
2/5/64 Tokaimura Depth = 54	$M_{JMA} = 6.0$ $M_L = 5.8$	KT001	36	65	North	3.50	6.15	5.78
					East	3.64	6.11	5.74
		KT001	36	65	North	4.02	6.67	6.3
					East	3.60	6.25	5.88
		KT001	36	65	North	3.31	6.06	5.59
					East	3.28	6.03	5.56
6/16/64 Niigata Depth = 40	$M_{JMA} = 7.5$ $M_L = 7.3$	Niigataph	59	57	North	4.63	7.2	7.22
					East	4.75	7.32	7.44
11/14/64 Depth = 69	$M_{JMA} = 5.1$ $M_L = 5.5$	KT001	8	69	North	3.78	6.47	5.45
					East	3.90	6.59	5.57
4/20/65 Depth = 40	$M_{JMA} = 6.1$ $M_L = 6.3$	CB002	21	45	North	4.30	6.72	6.3
					East	4.00	6.42	6.0
		CB057	30	50	S41E	4.19	6.68	6.37
					N49E	4.21	6.7	6.39

TABLE III (continued)

Earthquake		Site No.	Distance Epicentral	Distance Center of energy	Component	Log A_{wa}	$M_{L(CER)}$	$M_{L(EP)}$
10/26/65 Depth = 159	M_{JMA} = 7.1 M_L = 7.1	HK004	162	227	S15W	3.75	7.38	7.06
					S75E	3.74	7.37	7.05
4/5/66 Depth = 4	M_{JMA} = 5.4 M_L = 6.0	CB020	8	8	Transverse	4.12	5.75	5.75
					East	4.62	6.25	6.25
		CB020	12	12	North	4.67	6.47	6.47
					East	4.42	6.22	6.22
		Hoshira-A	3	5	North	4.19	5.76	5.69
					East	4.47	6.04	5.96
		Wakaho	4	6	North	4.45	6.05	5.98
					East	4.46	6.08	5.99
5/28/66 Depth = 10	M_{JMA} = 5.3 M_L = 5.2	CB056	7	12	North	3.50	5.3	5.13
					East	3.54	5.34	5.17
8/3/66 Depth = 3	M_{JMA} = 5.3 M_L = 6.1	Matsushiro	7	8	North	4.42	6.09	6.06
					East	4.52	6.19	6.16
11/12/66 Depth = 20	M_{JMA} = 5.9 M_L = 6.2	KS005	19	28	N40E	4.35	6.49	6.3
					N50W	4.24	6.38	6.19
11/19/67 Depth = 48	M_{JMA} = 6.0 M_L = 6.6	KT001	50	69	North	4.35	7.04	6.84
					East	3.94	6.63	6.43
3/30/68 Depth = 18	M_{JMA} = 5.0 M_L = 5.7	KK014	5	18	S10E	3.93	5.88	5.49
					N80E	4.26	6.21	5.82
4/1/68 Hyuganada Depth = 37	M_{JMA} = 7.5 M_L = 7.3	KS003	123	135	Longitude	3.71	6.85	6.82
					Transverse	3.77	6.91	6.88
		SK006	80	88	Longitude	4.44	7.32	7.24
					Transverse	4.62	7.50	7.42
		KS005	167	166	North	4.36	7.69	7.69
					East	4.48	7.81	7.81
		KS002	60	75	S30W	4.53	7.28	7.13
					S60E	4.76	7.51	7.36

TABLE III (continued)

Earthquake	Site No.	Distance Epicentral	Distance Center of energy	Component	Log A_{wa}	$M_{L(CER)}$	$M_{L(EP)}$
5/16/68 $M_{JMA}=7.9$ Tokachioki Depth = 10 $M_L=7.3$	HK009	276 (133)*	210	Longitude	4.63	8.18	7.79
				Transverse	4.68	8.23	7.84
	HK003	245 (112)	175	North	4.6	8.0	7.66
				East	4.4	7.8	7.46
	TH020	210 (107)	167	North	4.29	8.05	7.31
				East	4.67	8.01	7.7
	TH014	173 (123)	190	North	3.85	7.3	6.96
				East	3.80	7.25	6.91
	HK013	128 (50)	92	Longitude	3.91	6.83	6.42
				Transverse	3.87	6.79	6.38
	TH029	172 (96)	144	North	4.66	7.88	7.62
				East	4.74	7.96	7.7
5/16/68 $M_{JMA}=7.5$ Tokachioki aftershock Depth = 26 $M_L=7.0$	HK003	236	115	North	3.99	7.07	7.67
				East	4.00	7.08	7.68
	HK013	75	90	Longitude	3.63	6.53	6.38
				Transverse	3.72	6.62	6.47
	TH014	226	220	North	3.70	7.3	7.33
				East	3.60	7.2	7.23
5/23/68 $M_{JMA}=6.3$ Tokachioki Depth = 50 $M_L=6.4$	KS003	123	135	North	3.42	6.59	6.53
				East	3.27	6.44	6.38
7/1/68 $M_{JMA}=6.1$ Depth = 68 $M_L=6.9$	TK056	78	92	S3E	4.05	6.96	6.83
				N87E	4.20	7.11	6.98
7/5/68 $M_{JMA}=6.4$ Depth = 44 $M_L=6.5$	TH005	62	76	North	3.72	6.48	6.34
				East	3.95	6.71	6.57
8/6/68 $M_{JMA}=6.6$ Shikoku Depth = 48 $M_L=6.7$	CG005	116	106	North	3.77	6.8	6.8
				East	3.90	6.93	6.93
	SK006	14	54	Longitude	4.61	7.14	6.46
				Transverse	4.66	7.19	6.51
8/7/68 $M_{JMA}=5.7$ Hokkaido Depth = 68 $M_L=6.0$	HK004	32	75	North	3.71	6.46	5.91
				East	3.95	6.7	6.15

* Numbers in parentheses are closest-to-the-fault distances.

TABLE III (continued)

Earthquake	Site No.	Distance Epicentral	Distance Center of energy	Component	Log A_{wa}	$M_{L(CER)}$	$M_{L(EP)}$
10/8/68 $M_{JMA}=5.3$ South Honshu Depth = 73 $M_L=5.8$	KT004	38	82	North East	3.78 3.27	6.6 6.09	6.08 5.57
11/14/68 $M_{JMA}=6.0$ Depth = 40 $M_L=6.1$	TH014	83	92	North East	3.33 3.12	6.25 6.04	6.16 5.95
4/21/69 $M_{JMA}=6.5$ Kyushu Depth = 39 $M_L=6.4$	KS002	43	66	S30W S60E	4.0 3.95	6.66 6.61	6.4 6.35
9/9/69 $M_{JMA}=6.6$ South Honshu Depth = 29 $M_L=6.9$	AC017	101	103	North East	3.88 3.99	6.9 7.01	6.89 7.0
1/21/70 $M_{JMA}=6.6$ Hokkaido Depth = 25 $M_L=6.4$	HK013	46	51	Longitude Transverse	4.02 3.92	6.52 6.42	6.46 6.38
4/1/70 $M_{JMA}=5.8$ Depth = 75 $M_L=5.6$	TH014	17	77	North East	3.7 3.64	6.47 6.41	5.6 5.54
7/26/70 $M_{JMA}=6.7$ Kyushu Depth = 47 $M_L=6.3$	KS002	21	51	S30W S60E	2.26 2.30	6.76 6.8	6.26 6.3
	KS003	70	84	Longitude Transverse	3.56 3.63	6.4 6.47	6.33 6.33
7/26/70 $M_{JMA}=6.1$ Kyushu aftershock Depth = 47 $M_L=5.7$	KS002	21	51	S30W S60E	3.6 3.74	6.1 6.24	5.6 5.74
1/5/71 $M_{JMA}=6.1$ Depth = 44 $M_L=6.8$	KK026	64	78	North East	4.12 4.15	6.9 6.93	6.76 6.79
2/26/71 $M_{JMA}=5.5$ Depth = 37 $M_L=6.1$	CB030	27	46	Longitude Transverse	3.95 3.95	6.4 6.4	6.07 6.07
6/13/71 $M_{JMA}=5.3$ Depth = 55 $M_L=6.1$	KT001	35	65	North East	3.94 3.82	6.59 6.47	6.2 6.08
8/2/71 $M_{JMA}=7.0$ Hokkaido Depth = 45 $M_L=7.5$	HK004	196	201	S15W S75E	4.01 4.08	7.51 7.58	7.5 7.57
10/11/71 $M_{JMA}=5.2$ East Honshu Depth = 40 $M_L=5.6$	KT050	12	42	S29W S61E	3.42 4.13	5.8 6.51	5.22 5.93

TABLE III (continued)

Earthquake	Site No.	Distance Epicentral	Distance Center of energy	Component	Log A_{wa}	$M_{L(CER)}$	$M_{L(EP)}$
2/29/72 $M_{JMA}=7.1$ South Honshu Depth = 50 $M_L=7.3$	KT004	259	240	S33W	3.62	7.32	7.22
				S75E	3.70	7.4	7.3
5/11/72 $M_{JMA}=5.8$ Depth = 56 $M_L=6.1$	HK004	33	71	S15W	3.85	6.56	6.09
				S75E	3.88	6.59	6.12
6/17/73 $M_{JMA}=7.4$ Depth = 41 $M_L=7.6$	HK004	112	134	S15W	4.67	7.84	7.73
				S75E	4.41	7.58	7.47
11/19/73 $M_{JMA}=6.4$ Depth = 56 $M_L=6.6$	TH033	107	121	North	3.87	6.97	6.9
				East	3.37	6.47	6.4
3/3/74 $M_{JMA}=6.1$ East Honshu Depth = 49 $M_L=6.4$	KT036	39	63	North	3.92	6.59	6.25
				East	4.24	6.87	6.57
7/8/74 $M_{JMA}=6.3$ East Honshu Depth = 45 $M_L=6.5$	KT036	73	87	North	3.78	6.65	6.51
				East	3.72	6.59	6.45
9/4/74 $M_{JMA}=5.6$ Depth = 52 $M_L=6.1$	TH029	42	67	North	3.76	6.43	6.15
				East	3.74	6.45	6.13
11/9/74 $M_{JMA}=6.5$ Hokkaido Depth = 125 $M_L=5.7$	HK016	15	126	S83	3.72	6.85	5.6
				N92E	3.85	6.98	5.73
11/16/74 $M_{JMA}=6.1$ East Honshu Depth = 44 $M_L=6.4$	KT036	38	58	North	4.18	6.76	6.5
				East	3.97	6.55	6.29
6/12/78 $M_{JMA}=7.5$ Sendai Depth = 40 $M_L=7.5$	TH019	116	102	N41E	4.24	7.25	7.32
				S49E	4.23	7.24	7.31
	TH033	120	102	North	4.69	7.7	7.79
				East	4.95	7.96	8.05

magnitudes and source distance, we see that the Japanese and U.S. motions are remarkably similar (Figure 19 c through h; Figure 20 c through h; Figure 21 c through h). We see then that the primary reason that the distribution for peak values with distance for the entire U.S. and Japanese data sets are different is mainly geometry. That is, there are many near-source recordings of moderate-sized U.S. earthquakes, but earthquakes of $M > 7$ have been rare. In contrast, there are numerous recordings of large Japanese earthquakes, but very near-source records are rare. This is due to the fact that most large Japanese earthquakes occur offshore along subduction zones.

We have superposed the modified local magnitude distance attenuation law (shown in Figure 8) on these plots. We see that the distance decay of peak ground motions

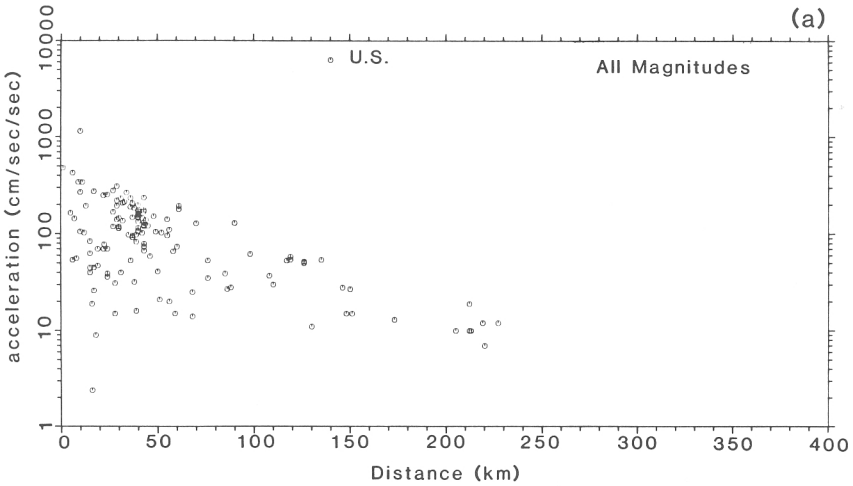
(a)
U.S.
All Magnitudes
acceleration (cm/sec/sec)
10000
1000
100
10
1
0
50
100
150
200
250
300
350
400
Distance (km)

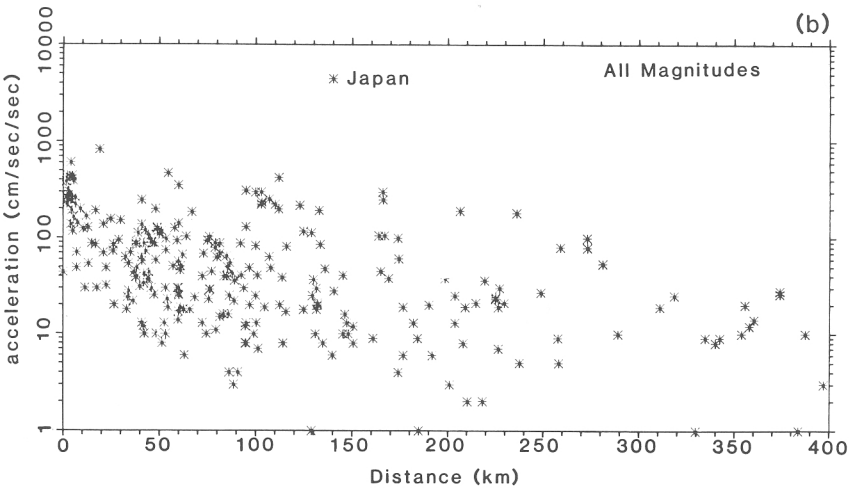
(b)
Japan
All Magnitudes
acceleration (cm/sec/sec)
10000
1000
100
10
1
0
50
100
150
200
250
300
350
400
Distance (km)

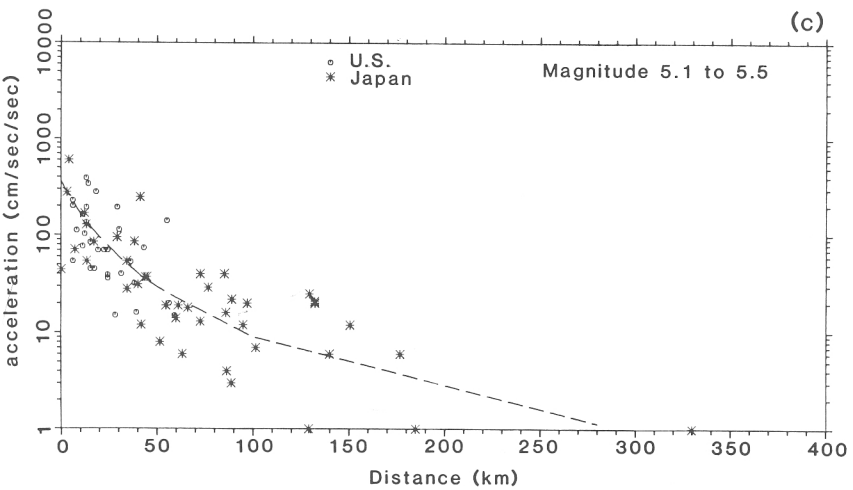
(c)
U.S.
Japan
Magnitude 5.1 to 5.5
acceleration (cm/sec/sec)
10000
1000
100
10
1
0
50
100
150
200
250
300
350
400
Distance (km)

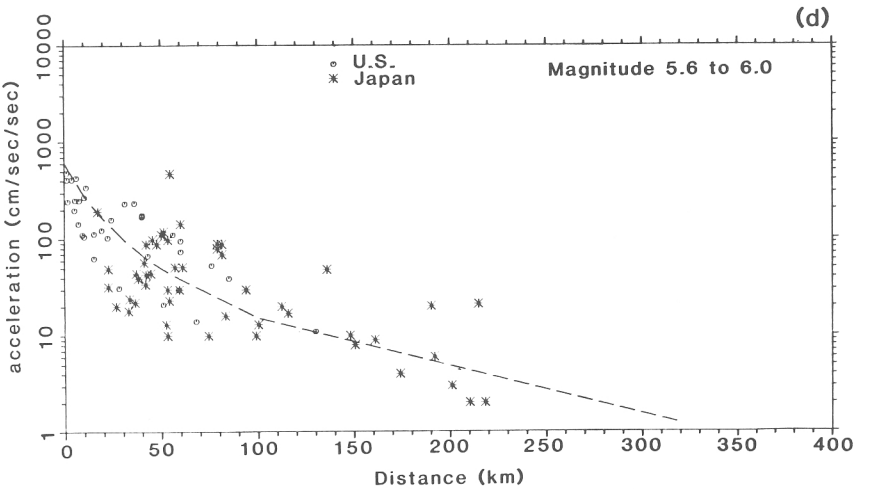
(d)
U.S.
Japan
Magnitude 5.6 to 6.0
acceleration (cm/sec/sec)
10000
1000
100
10
1
0
50
100
150
200
250
300
350
400
Distance (km)

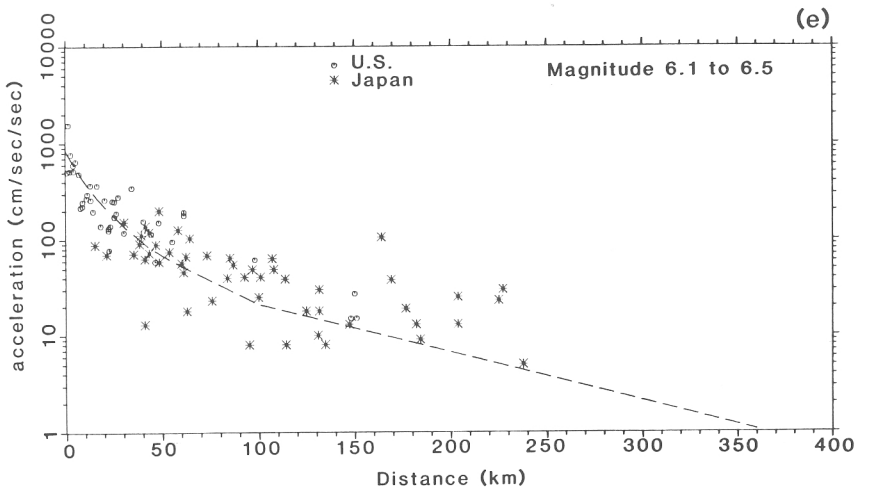
(e)
U.S.
Japan
Magnitude 6.1 to 6.5
acceleration (cm/sec/sec)
10000
1000
100
10
1
0
50
100
150
200
250
300
350
400
Distance (km)

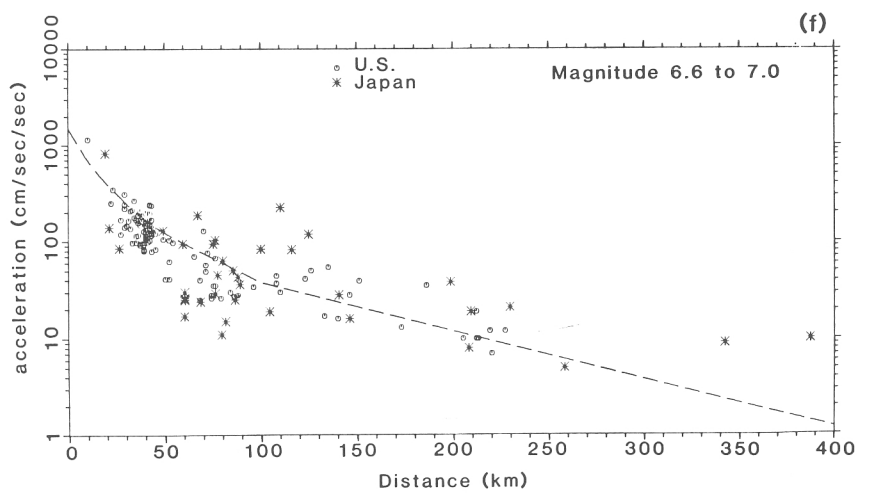
(f)
U.S.
Japan
Magnitude 6.6 to 7.0
acceleration (cm/sec/sec)
10000
1000
100
10
1
0
50
100
150
200
250
300
350
400
Distance (km)

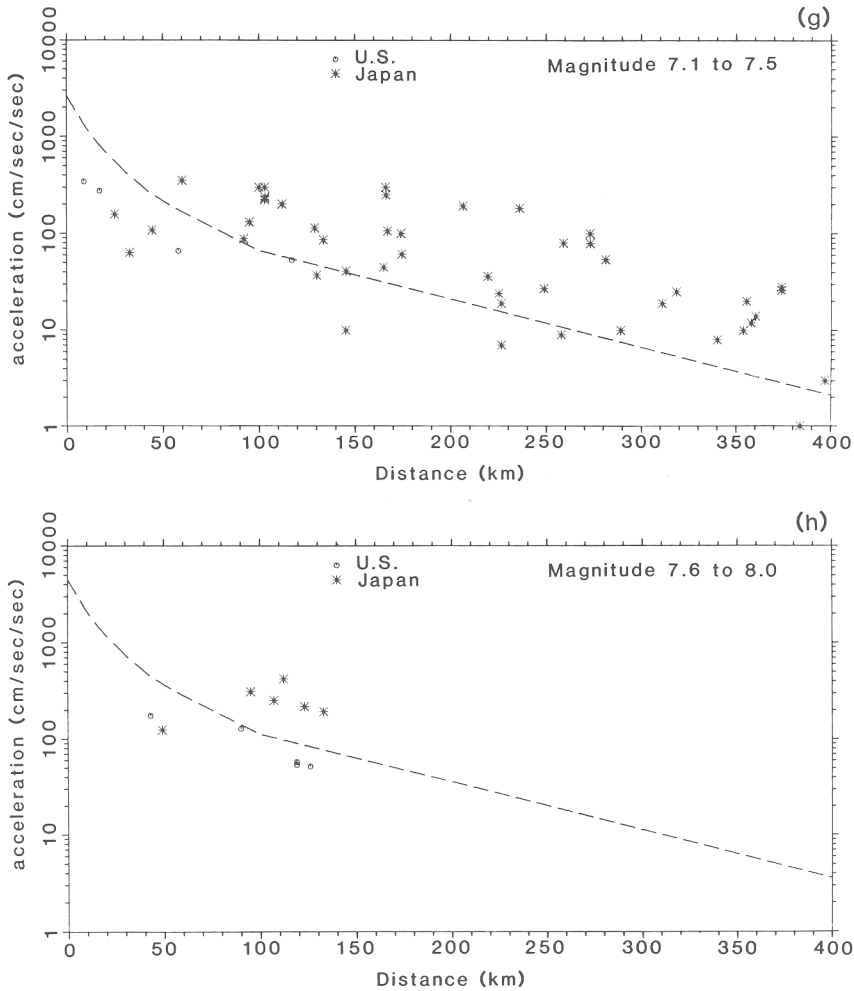

Fig. 19. Comparison of peak ground accelerations recorded in the western U.S. and Japan. Distance is approximately the closest horizontal distance to the rupture. Dashed line is the modified local magnitude distance attenuation law (Table I).

recorded in both Japan and the U.S. is compatible with the local magnitude attenuation law. This is somewhat surprising considering the wide range of earthquake sizes and tectonic settings being compared. However, if this attenuation law is applied to earthquakes of $M > 7$, then we obtain very large near-source ground motions (peak velocities in excess of 500 cm sec^{-1}). Since there is really no data taken very close to very large earthquakes, it is difficult to assess the validity of the local magnitude distance scaling law for very large earthquakes at small source distances. Nevertheless, we feel that the distance attenuation law is likely to change as the source dimension becomes large relative to the recording distance. Furthermore, in such cases, the distance attenuation is probably a function of the fault length to width ratio and we expect near-

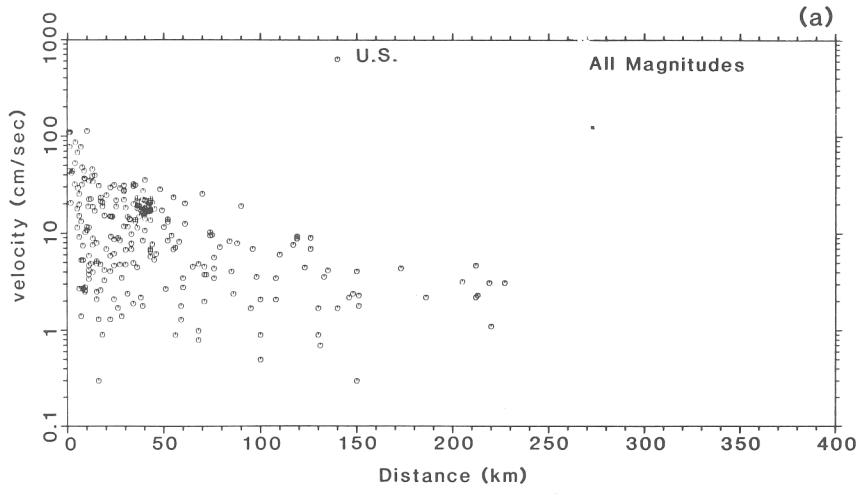
(a)
U.S.
All Magnitudes
velocity (cm/sec)
1000
100
10
1
0.1
0
50
100
150
200
250
300
350
400
Distance (km)

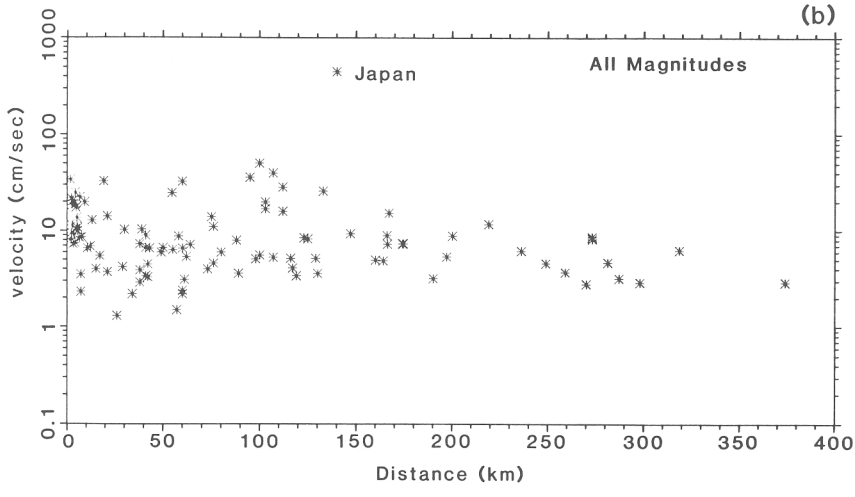
(b)
Japan
All Magnitudes
velocity (cm/sec)
1000
100
10
1
0.1
0
50
100
150
200
250
300
350
400
Distance (km)

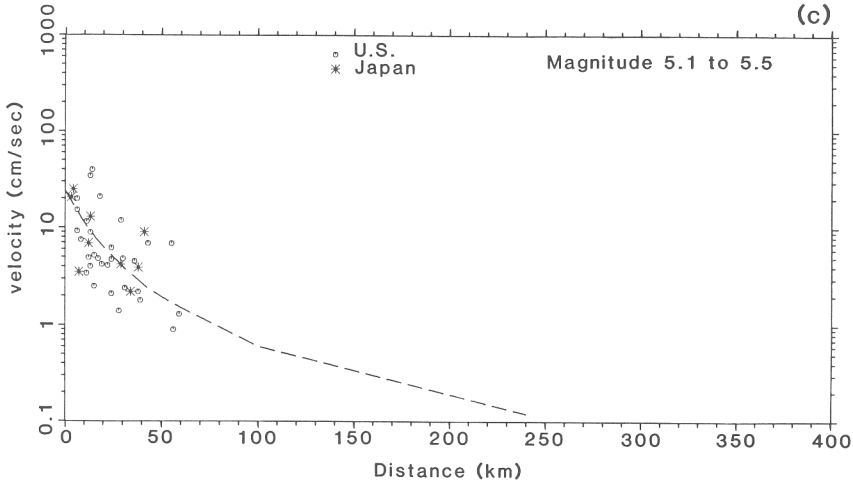
(c)
U.S.
Japan
Magnitude 5.1 to 5.5
velocity (cm/sec)
1000
100
10
1
0.1
0
50
100
150
200
250
300
350
400
Distance (km)

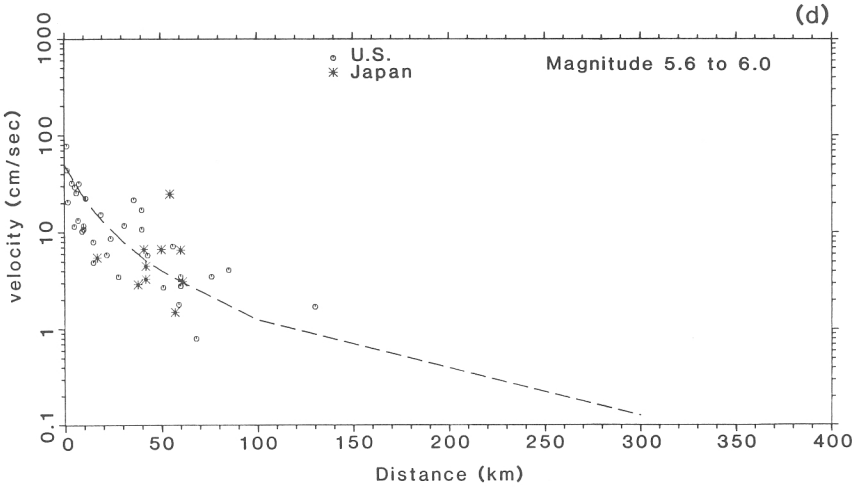
(d)
U.S.
Japan
Magnitude 5.6 to 6.0
velocity (cm/sec)
1000
100
10
1
0.1
0
50
100
150
200
250
300
350
400
Distance (km)

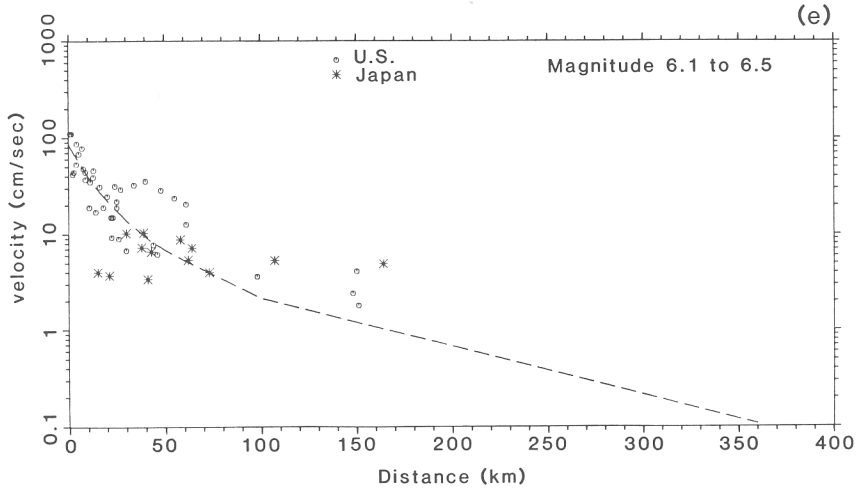
(e)
U.S.
Japan
Magnitude 6.1 to 6.5
velocity (cm/sec)
1000
100
10
1
0.1
0
50
100
150
200
250
300
350
400
Distance (km)

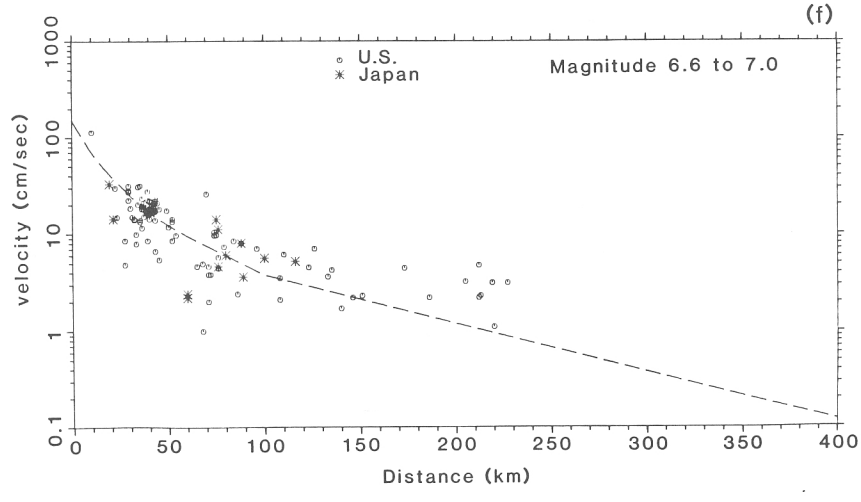
(f)
U.S.
Japan
Magnitude 6.6 to 7.0
velocity (cm/sec)
1000
100
10
1
0.1
0
50
100
150
200
250
300
350
400
Distance (km)

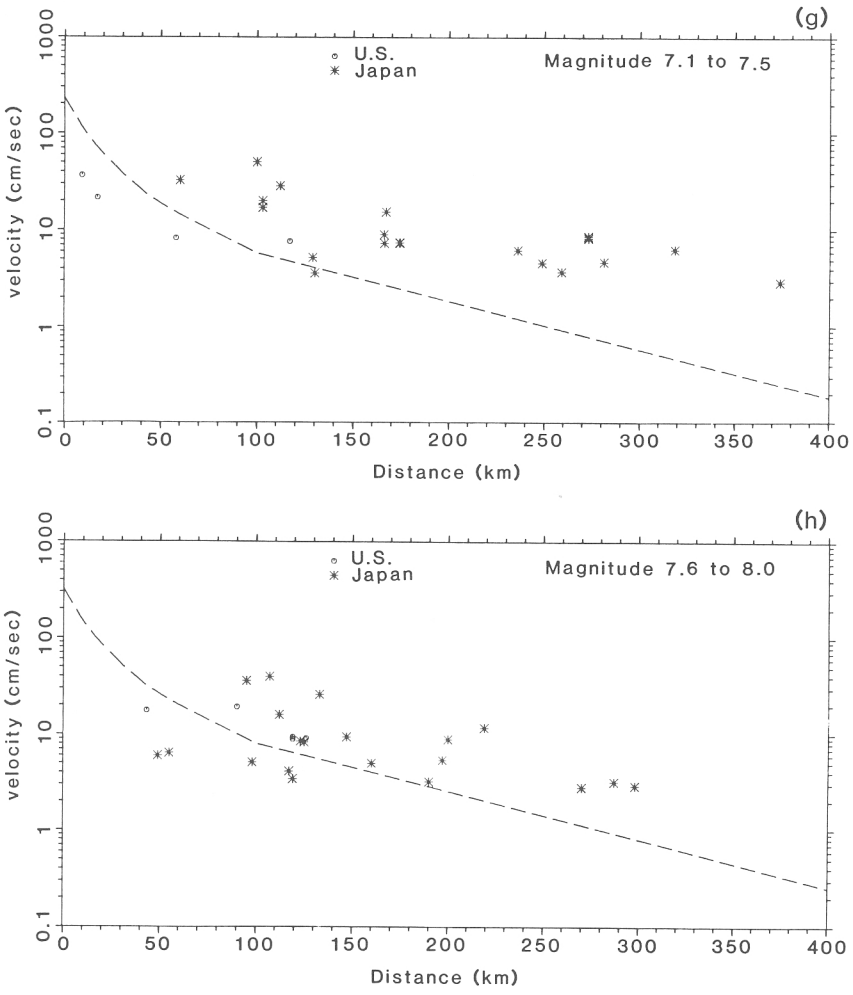

Fig. 20. Comparison of peak ground velocities recorded in the western U.S. and Japan.

source attenuation from subduction zone earthquakes to be different from attenuation close to shallow crustal earthquakes.

We have also calculated local magnitudes for 75 Japanese earthquakes using 138 horizontal accelerograph traces given in the catalogue of Mori and Crouse (1981). Following the method of Kanamori and Jennings (1978), we created Wood-Anderson seismograms by convolving processed accelerogram data with the theoretical instrument response of a Wood-Anderson seismometer. The modified distance attenuation was then used to compute the local magnitudes which are given in Table III. Local magnitudes are given assuming both center of energy distance and closest horizontal distance to the rupture. In most cases, these translate into hypocentral distance and epicentral distance, respectively.

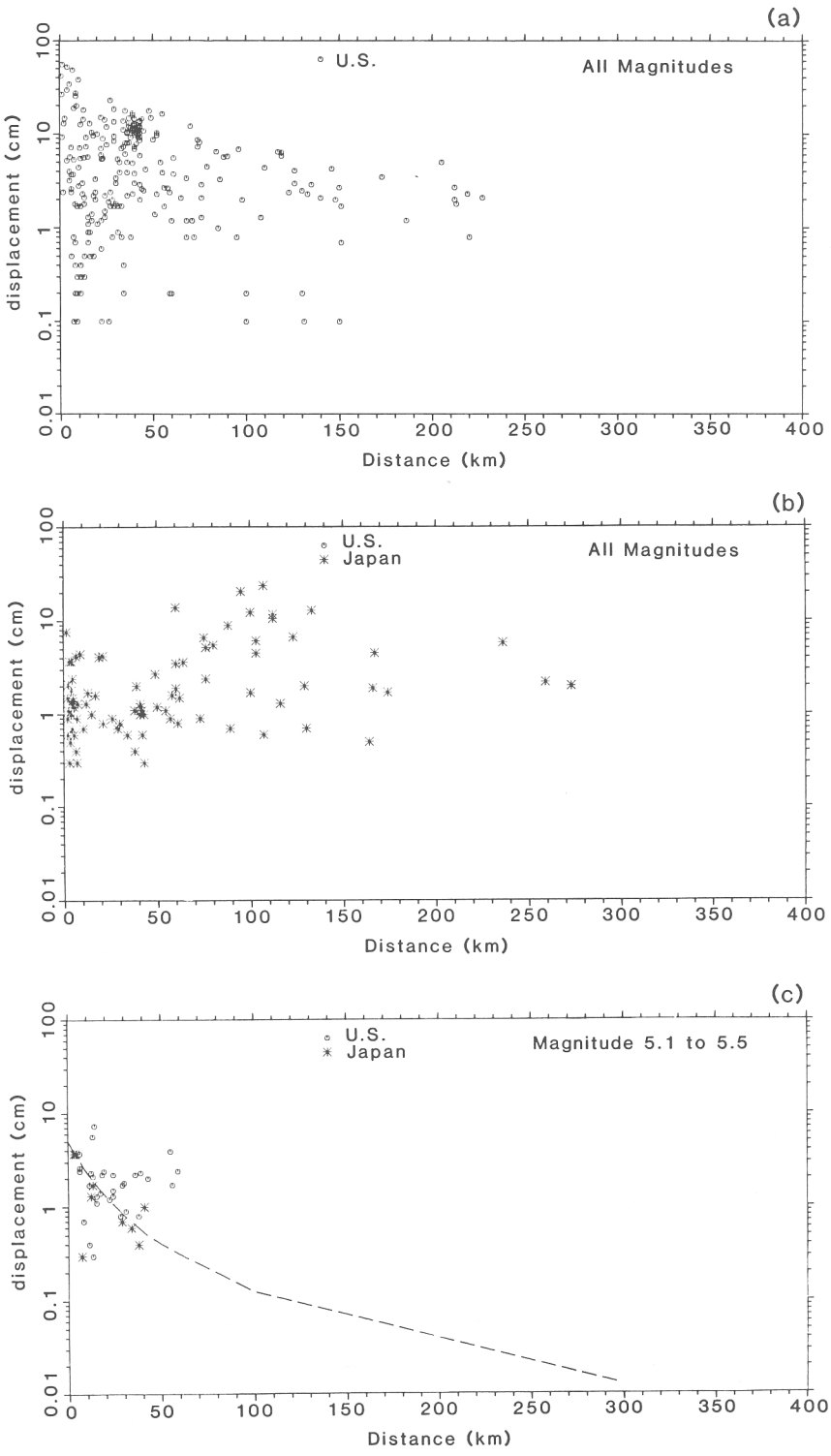
(a)
U.S.
All Magnitudes
displacement (cm)
0.01
0.1
1
10
100
0
50
100
150
200
250
300
350
400
Distance (km)
(b)
U.S.
Japan
All Magnitudes
displacement (cm)
Distance (km)
(c)
U.S.
Japan
Magnitude 5.1 to 5.5
displacement (cm)
Distance (km)

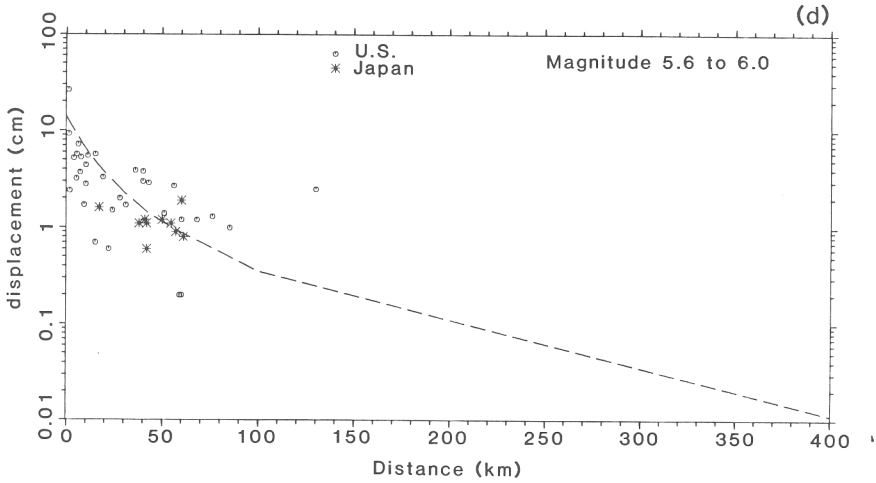
(d)
U.S.
Japan
Magnitude 5.6 to 6.0
displacement (cm)
0.01
0.1
1
10
100
0
50
100
150
200
250
300
350
400
Distance (km)

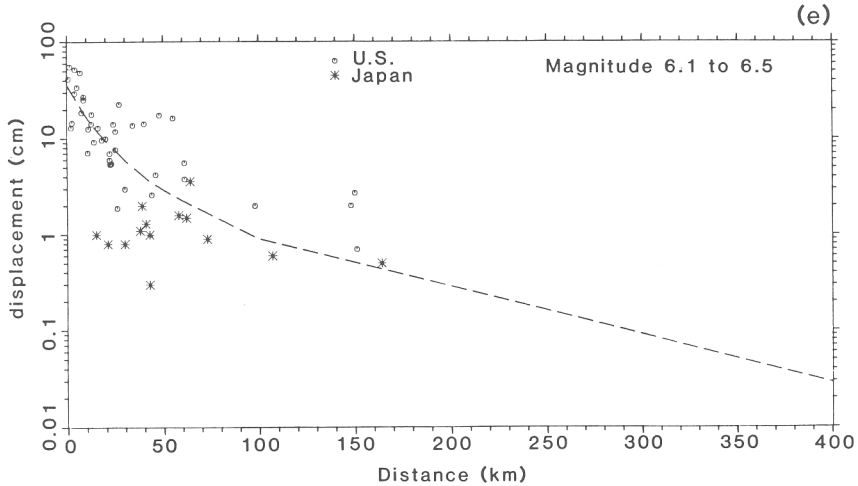
(e)
U.S.
Japan
Magnitude 6.1 to 6.5
displacement (cm)
0.01
0.1
1
10
100
0
50
100
150
200
250
300
350
400
Distance (km)

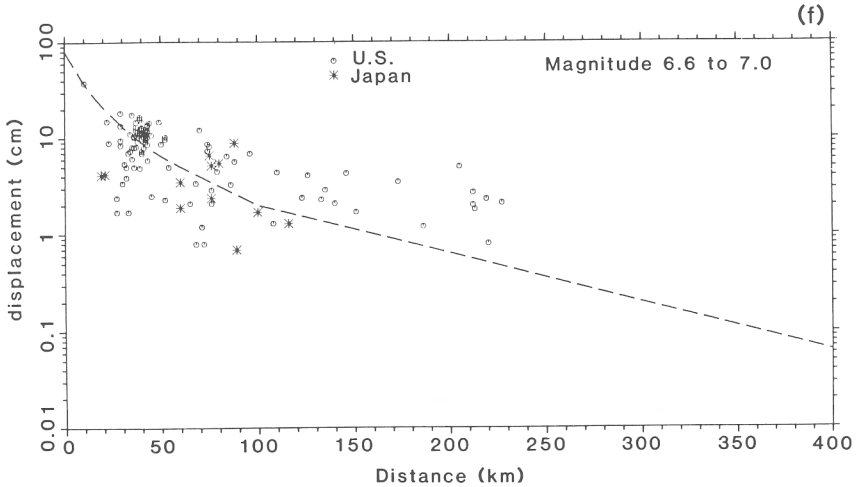
(f)
U.S.
Japan
Magnitude 6.6 to 7.0
displacement (cm)
0.01
0.1
1
10
100
0
50
100
150
200
250
300
350
400
Distance (km)

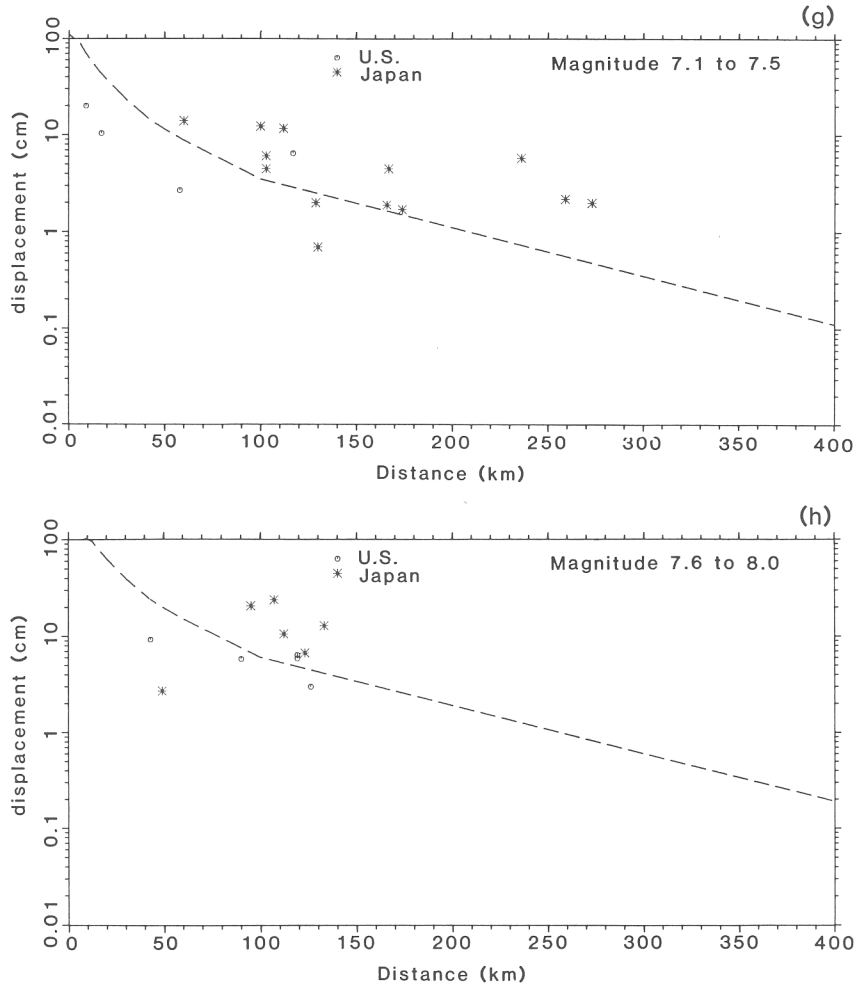

Fig. 21. Comparison of peak ground displacements recorded in the western U.S. and Japan.

In Figure 22, we have plotted each Japanese earthquake for which we have estimates of both local magnitude and JMA magnitude. In this figure, local magnitudes were determined using the closest horizontal distance to the rupture. JMA magnitude has been determined by the Japan Meteorological Agency using long-period local seismometers (distances of less than 1000 km) and is similar in many respects to surface wave magnitude. We see that the relationship between M_L and M_{JMA} for Japanese earthquakes is similar to that found between M_L and M_s for earthquakes in the western U.S. (Figure 4).